PDGFRα signaling regulates Srsf3 transcript binding to affect PI3K signaling and endosomal trafficking

Thomas E. Forman[1,2], Marcin P. Sajek[3,4,5], Eric D. Larson[6,7], Neelanjan Mukherjee[3,4], Katherine A. Fantauzzo[1,4,*]

[1]Department of Craniofacial Biology, School of Dental Medicine, University of Colorado Anschutz Medical Campus, Aurora, CO, USA

[2]Medical Scientist Training Program, University of Colorado Anschutz Medical Campus, Aurora, CO, USA

[3]Department of Biochemistry and Molecular Genetics, School of Medicine, University of Colorado Anschutz Medical Campus, Aurora, CO, USA

[4]RNA Bioscience Initiative, University of Colorado Anschutz Medical Campus, Aurora, CO, USA

[5]Institute of Human Genetics, Polish Academy of Sciences, Poznan, Poland

[6]Department of Otolaryngology – Head and Neck Surgery, University of Colorado Anschutz Medical Campus, Aurora, CO, USA

[7]Basic and Translational Sciences, Penn Dental Medicine, University of Pennsylvania, Philadelphia, PA, USA

*Corresponding author. Email: katherine.fantauzzo@cuanschutz.edu

Abstract

Signaling through the platelet-derived growth factor receptor alpha (PDGFRα) plays a critical role in craniofacial development, as mutations in *PDGFRA* are associated with cleft lip/palate in humans and *Pdgfra* mutant mouse models display varying degrees of facial clefting. Phosphatidylinositol 3-kinase (PI3K)/Akt is the primary effector of PDGFRα signaling during skeletal development in the mouse. We previously demonstrated that Akt phosphorylates the RNA-binding protein serine/arginine-rich splicing factor 3 (Srsf3) downstream of PI3K-mediated PDGFRα signaling in mouse embryonic palatal mesenchyme (MEPM) cells, leading to its nuclear translocation. We further showed that ablation of *Srsf3* in the murine neural crest lineage results in severe midline facial clefting, due to defects in proliferation and survival of cranial neural crest cells, and widespread alternative RNA splicing (AS) changes. Here, we sought to determine the molecular mechanisms by which Srsf3 activity is regulated downstream of PDGFRα signaling to control AS of transcripts necessary for craniofacial development. We demonstrated via enhanced UV-crosslinking and immunoprecipitation (eCLIP) of MEPM cells that PDGF-AA stimulation leads to preferential binding of Srsf3 to exons and loss of binding to canonical Srsf3 CA-rich motifs. Through the analysis of complementary RNA-seq data, we showed that Srsf3 activity results in the preferential inclusion of exons with increased GC content and lower intron to exon length ratio. Moreover, we found that the subset of transcripts that are bound by Srsf3 and undergo AS upon PDGFRα signaling commonly encode regulators of PI3K signaling and early endosomal trafficking. Functional validation studies further confirmed that Srsf3 activity downstream of PDGFRα signaling leads to retention of the receptor in early endosomes and increases in downstream PI3K-mediated Akt signaling. Taken together, our findings reveal that growth factor-mediated phosphorylation of an RNA-binding protein underlies gene expression regulation necessary for mammalian craniofacial development.

Introduction

Craniofacial development is a complex morphogenetic process that requires a precise interplay of multiple cell and tissue types to generate the frontonasal skeleton. Disruption of this process can result in some of the most common birth differences in humans, such as cleft lip and palate (Mai et al., 2019). Signaling through the platelet derived growth factor receptor alpha (PDGFRα) receptor tyrosine kinase (RTK) is essential for human craniofacial development. Heterozygous missense mutations in the coding region of *PDGFRA* that alter amino acids within the extracellular, transmembrane or cytoplasmic domains of the receptor, in addition to single base-pair substitutions in the 3' untranslated region (3' UTR), are associated with nonsyndromic cleft palate (Rattanasopha et al., 2012). Further, single-nucleotide polymorphisms that repress transcriptional activity of the promoter upstream of *PDGFC*, which encodes one of two PDGFRα ligands, are associated with cleft lip and palate (Choi et al., 2009). This role of PDGFRα signaling in craniofacial development is conserved in mice, as *Pdgfra* mutant mouse models display a variety of defects that range from cleft palate to complete facial clefting (Klinghoffer et al., 2002; Soriano, 1997; Tallquist & Soriano, 2003; Fantauzzo & Soriano, 2014; He & Soriano, 2013). These phenotypes are recapitulated in embryos lacking both *Pdgfa* and *Pdgfc* (Ding et al., 2004). Phosphatidylinositol 3-kinase (PI3K) is the primary effector of PDGFRα signaling during skeletal development in the mouse (Klinghoffer et al., 2002). Following activation, PI3K increases phosphatidylinositol-3,4,5-trisphosphate (PIP_3) levels at the cell membrane, leading to the recruitment and subsequent phosphorylation of the serine/threonine kinase Akt. Akt subsequently dissociates from the membrane to phosphorylate an array of target proteins that are involved in wide-ranging cellular processes (Manning & Cantley, 2007). We previously identified proteins phosphorylated by Akt downstream of PI3K-mediated PDGFRα signaling in primary mouse embryonic mesenchyme (MEPM) cells (Fantauzzo & Soriano, 2014). Gene

ontology analysis revealed that 25% of the 56 proteins were involved in RNA processing, with a particular enrichment for RNA splicing (Fantauzzo & Soriano, 2014).

Alternative RNA splicing (AS) is a process by which different combinations of exons from the same gene are incorporated into mature RNA transcripts, thereby contributing to gene expression regulation and enhancing the diversity of protein isoforms (Licatalosi & Darnell, 2010). AS occurs in approximately 95% of multi-exon human genes, frequently in a tissue-specific manner (Pan et al., 2008; Wang et al., 2008). Dysregulation of AS causes a number of diseases due to mutations in precursor RNA sequences, mutations in core components of the spliceosome complex and/or mutations in auxiliary RNA-binding proteins (RBPs) (Scotti & Swanson, 2016). These *trans*-acting auxiliary RBPs bind to specific sequence and/or structural motifs in a target RNA via one or more RNA-binding domains to promote or inhibit exon inclusion (Fu & Ares, 2014; Licatalosi & Darnell, 2010). The phenotypes resulting from global and/or tissue-specific knockout of multiple RBPs have established that RBP-mediated AS is an essential process during mouse craniofacial development (Bebee et al., 2015; Cibi et al., 2019; Dennison et al., 2021; Forman et al., 2021; Lee et al., 2020). We previously demonstrated that ablation of *Srsf3* in the murine neural crest lineage results in severe midline facial clefting and facial bone hypoplasia, due to defects in proliferation and survival of cranial neural crest cells, and widespread AS changes (Dennison et al., 2021).

Srsf3 belongs to the serine/arginine-rich (SR) protein family of splicing factors that generally promote exon inclusion by binding to exonic and intronic splicing enhancers and by recruiting spliceosome components to the 5' and 3' splice sites (Fu & Ares, 2014; Licatalosi & Darnell, 2010). Srsf3 specifically was shown to bind pyrimidine-rich motifs, with a preference for exonic regions (Akerman et al., 2009; Änkö et al., 2012). Srsf3 is phosphorylated downstream of PDGF and EGF stimulation and all-*trans* retinoic acid treatment, and by the kinases Akt and SRPK2 (Bavelloni et al., 2014; Dennison et al., 2021; Fantauzzo & Soriano, 2014; Long et al., 2019; Zhou et al., 2012). Phosphorylation of the Akt consensus sites within the C-terminal

arginine/serine-rich (RS) domain of Srsf3 drives its translocation to the nucleus, where AS takes place (Bavelloni et al., 2014; Dennison et al., 2021; Long et al., 2019). Moreover, phosphorylation of the RS domain can alter the ability of SR proteins to interact with other proteins, such as the U1 small nuclear ribonucleoprotein (snRNP) component of the spliceosome and additional RBPs, and affect the ability of SR proteins to bind RNA (Huang et al., 2004; Shen & Green, 2006; Shin et al., 2004; Xiao & Manley, 1997). However, the molecular mechanisms by which Srsf3 activity is regulated downstream of specific signaling inputs in a context-specific manner to regulate RNA binding and/or sequence specificity remain undetermined.

Here, we identified changes in Srsf3-dependent AS and Srsf3 transcript binding in the absence or presence of PDGF-AA ligand in MEPM cells. RNA-sequencing (RNA-seq) analysis revealed that Srsf3 activity and PDGFRα signaling have more pronounced effects on AS than gene expression, as well as a significant dependence in regulating AS. Using enhanced UV-crosslinking and immunoprecipitation (eCLIP), we found a shift from intronic to exonic Srsf3 binding and loss of CA-rich sites upon PDGF-AA stimulation. Further, we demonstrated that the subset of transcripts that are bound by Srsf3 and undergo AS upon PDGFRα signaling commonly encode regulators of PI3K signaling and early endosomal trafficking, ultimately serving as a feedback mechanism to affect trafficking of the receptors. Combined, our findings provide significant insight into the mechanisms underlying RBP-mediated gene expression regulation in response to growth factor stimulation within the embryonic mesenchyme.

Results

PDGFRα signaling for one hour minimally affects gene expression

To determine the Srsf3-dependent changes in gene expression and AS downstream of PDGFRα signaling, we stably integrated a scramble shRNA (scramble) or an shRNA targeting

the 3' UTR of *Srsf3* (shSrsf3) into immortalized MEPM (iMEPM) cells via lentiviral transduction (Fig. 1A). Western blotting revealed a 66% decrease in Srsf3 protein levels in the shSrsf3 cell line (Fig. 1B). We previously demonstrated that phosphorylated Srsf3 levels peaked in the nucleus of iMEPM cells following 1 hour of PDGF-AA ligand treatment (Dennison et al., 2021). As such, cells were left unstimulated (-PDGF-AA) or treated with 10 ng/mL PDGF-AA for 1 hour (+PDGF-AA). RNA was isolated and sequenced from three biological replicates across each of the four conditions (Fig. 1A; Table S1). We first examined Srsf3-dependent differentially-expressed (DE) genes by comparing scramble versus shSrsf3 samples across the same PDGF-AA stimulation condition (-PDGF-AA or +PDGF-AA). We detected 827 DE genes in the absence of ligand treatment and 802 DE genes upon ligand stimulation (Fig. 1C, Table S2). There was extensive overlap (521 out of 1,108; 47.0%) of Srsf3-dependent DE genes across ligand treatment conditions, resulting in a total of 1,108 unique genes within both datasets (Fig. 1C,D; Fig. S1A). Of the 521 shared DE genes, 514 (98.7%) had the same directionality, including 273 (52%) with shared increases in expression in the shSrsf3 samples and 241 (46%) with shared decreases in expression in the shSrsf3 samples (Fig. 1C,D). These findings demonstrate that expression of a set of genes (521) depends on Srsf3 activity independent of PDGFRα signaling, while a similarly sized set of genes (587) is differentially expressed in response to both Srsf3 activity and PDGFRα signaling (Fig. 1C,D). Gene ontology (GO) analysis of the Srsf3-dependent DE genes revealed that the most significant terms for biological process commonly involved regulation of osteoblast differentiation, calcium-dependent cell-cell adhesion, regulation of cell migration and canonical Wnt signaling, while only a handful of significant terms for molecular function were detected in unstimulated cells, relating to cation channel activity and phosphatase activity (Fig. S2A,B).

We next examined PDGF-AA-dependent DE genes by comparing -PDGF-AA versus +PDGF-AA across the same Srsf3 condition (scramble or shSrsf3). We detected only 37 DE

145 genes in scramble cells and 14 DE genes in shSrsf3 cells (Fig. 1E, Table S2). There was limited
146 overlap (4 out of 47; 8.51%) of PDGF-AA-dependent DE genes across Srsf3 conditions,
147 resulting in a total of 47 unique genes within both datasets (Fig. 1E,F; Fig. S1B). Of the 4
148 shared DE genes, 3 (75%) had shared increases in expression upon PDGF-AA stimulation (Fig.
149 1E,F). These findings demonstrate that, unlike Srsf3 activity, PDGFRα signaling minimally
150 affects gene expression at one hour of ligand stimulation, consistent with our previous findings
151 in mouse embryonic facial mesenchyme (Dennison et al., 2021). Further, these results show
152 that expression of a set of genes (4) depends on PDGFRα signaling independent of Srsf3
153 activity, while a larger set of genes (43) is differentially expressed in response to both PDGFRα
154 signaling and Srsf3 activity (Fig. 1E,F). GO analysis of the PDGF-AA-dependent DE genes
155 revealed significant terms for biological process in the scramble cells relating to cell migration,
156 response to growth factor stimulation and regulation of transcription (Fig. S2A). The most
157 significant terms for molecular function commonly involved DNA binding (Fig. S2B).
158
159 *PDGFRα signaling for one hour has a more pronounced effect on alternative RNA splicing*
160 We previously demonstrated that AS is an important mechanism of gene expression
161 regulation downstream of PI3K/Akt-mediated PDGFRα signaling in the murine mid-gestation
162 palatal shelves (Dennison et al., 2021). Accordingly, we next assessed AS in our same RNA-
163 seq dataset. In examining Srsf3-dependent alternatively-spliced transcripts, we detected 1,354
164 differential AS events in the absence of ligand treatment and 1,071 differential AS events upon
165 ligand stimulation (Fig. 2A). When filtered to include events detected in at least 10 reads in
166 either condition, we obtained a list of 1,113 differential AS events in the absence of ligand
167 treatment and 795 differential AS events upon ligand stimulation (Fig. 2B, Tables S3 and S4).
168 There was limited overlap (203 out of 1,705; 11.9%) of Srsf3-dependent alternatively-spliced
169 transcripts across ligand treatment conditions, resulting in a total of 1,705 unique events within

both datasets (Fig. 2A,B). Of the 203 shared alternatively-spliced transcripts, 100% had the same directionality, including 81 (40%) with shared negative changes in percent spliced in (PSI) (exon included more often in shSrsf3 samples) and 122 (60%) with shared positive changes in PSI (exon skipped more often in shSrsf3 samples) (Fig. 2A,B). We confirmed the differential AS of two transcripts, *Arhgap12* and *Cep55*, between scramble and shSrsf3 samples by qPCR using primers within constitutively-expressed exons flanking the alternatively-spliced exon (Fig. S3A,B). These findings demonstrate that AS of a set of transcripts (203) depends on Srsf3 activity independent of PDGFRα signaling, while a much larger set of transcripts (1,502) is alternatively spliced in response to both Srsf3 activity and PDGFRα signaling (Fig. 2A,B). GO analysis of these Srsf3-dependent alternatively-spliced transcripts revealed that the most significant terms for biological process and molecular function commonly involved regulation of RNA splicing, and RNA binding and cadherin binding, respectively (Fig. S4A,B).

In examining PDGF-AA-dependent alternatively-spliced transcripts, we detected 595 differential AS events in scramble cells and 398 differential AS events in shSrsf3 cells (Fig. 2C). When filtered to include events detected in at least 10 reads in either condition, we obtained a list of 375 differential AS events in scramble cells and 256 differential AS events in shSrsf3 cells (Fig. 2D, Tables S5 and S6). There was negligible overlap (9 out of 622; 1.45%) of PDGF-AA-dependent alternatively-spliced transcripts across Srsf3 conditions, resulting in a total of 622 unique events within both datasets (Fig. 2C,D). Of the 9 shared alternatively-spliced transcripts, 100% had the same directionality, including 5 (56%) with shared negative changes in PSI (exon included more often in +PDGF-AA samples) and 4 (44%) with shared positive changes in PSI (exon skipped more often in +PDGF-AA samples) (Fig. 2C,D). Taken together, these findings demonstrate that both Srsf3 activity and PDGFRα signaling have more pronounced effects on AS than gene expression. While more transcripts and genes are subject to these regulatory mechanisms upon loss of Srsf3 activity, the magnitude of events is more greatly skewed

195 towards AS upon PDGF-AA stimulation. Further, these results show that AS of a set of
196 transcripts (9) depends on PDGFRα signaling independent of Srsf3 activity, while a much larger
197 set of transcripts (613) is alternatively spliced in response to both PDGFRα signaling and Srsf3
198 activity (Fig. 2C,D). When combined with the data above (Fig. 2B), this points to a profound
199 dependence between PDGFRα signaling and Srsf3 in regulating AS of transcripts in the facial
200 mesenchyme. GO analysis of these PDGF-AA-dependent alternatively-spliced transcripts
201 demonstrated only a handful of significant terms for molecular function in the scramble cells, all
202 relating to protein kinase activity (Fig. S4B).
203 The vast majority of Srsf3-dependent (70.2-73.7%) and PDGF-AA dependent (62.1-
204 65.1%) AS events involved skipped exons, with minimal contribution from retained introns,
205 mutually exclusive exons, alternative 5' splice sites, or alternative 3' splice sites (Fig. 2E). For
206 the Srsf3-dependent skipped exon events, there were more transcripts with +ΔPSI (exon
207 skipped more often in shSrsf3 samples) (44.8%) as opposed to -ΔPSI (exon included more
208 often in shSrsf3 samples) (25.4%) in the absence of PDGF-AA stimulation (Fig. 2E), consistent
209 with previous results that SR proteins tend to promote exon inclusion (Fu & Ares, 2014;
210 Licatalosi & Darnell, 2010). However, PDGF-AA ligand treatment led to an increase in the
211 percentage of transcripts with -ΔPSI (36.5%) (Fig. 2E), indicating that PDGFRα signaling
212 promotes exon skipping in the presence of Srsf3. Among the PDGF-AA-dependent skipped
213 exon events, there was a significant shift in transcripts with -ΔPSI (exon included more often in
214 +PDGF-AA samples) in the absence (41.0%) versus presence (19.5%) of Srsf3, and a
215 corresponding shift in transcripts with +ΔPSI (exon skipped more often in +PDGF-AA samples)
216 (21.1% and 45.6%, respectively) (Fig. 2E), again suggesting that PDGF-AA stimulation causes
217 increased exon skipping when Srsf3 is present.
218
219 *Srsf3 exhibits differential transcript binding upon PDGFRα signaling*

To determine direct binding targets of Srsf3 downstream of PDGFRα signaling, we conducted eCLIP (Van Nostrand et al., 2016, 2017) of iMEPM cells that were left unstimulated (-PDGF-AA) or treated with 10 ng/mL PDGF-AA for 1 hour (+PDGF-AA) as above (Fig. 3A; Table S7). Immunoprecipitation with a previously validated Srsf3 antibody (Dennison et al., 2021) successfully enriched for Srsf3 in UV-crosslinked cells (Fig. 3B). We detected 6,555 total eCLIP peaks in protein-coding genes in the -PDGF-AA samples and 8,584 total peaks in the +PDGF-AA samples (Table S8). Among the -PDGF-AA peaks, 3,727 (56.9%) were located in exons (CDS) and 1,690 (25.8%) were located within introns, with the rest binding within 5' UTRs (768, 11.7%) and 3' UTRs (367, 5.60%) (Fig. 3C,D; Table S9). We observed substantial shifts in Srsf3-bound regions upon PDGF-AA stimulation. Many more +PDGF-AA peaks were located within exons (7,139, 83.2%), and less were located within introns (765, 8.91%), 5' UTRs (389, 4.53%) and 3' UTRs (287, 3.34%) (Fig. 3C,D; Table S9). Given that SR proteins are crucial for exon definition and bind to exonic splicing enhancers to recruit and stabilize core splicing machinery (Fu & Maniatis, 1990; Krainer et al., 1991; Zahler et al., 1993), we investigated Srsf3 binding around 5' and 3' splice sites in response to PDGFRα signaling. Consistent with the results above and previous findings (Änkö et al., 2012), Srsf3 binding was enriched in exonic regions, as opposed to intronic regions, surrounding the splice sites (Fig. 3E). There was greater mean coverage of Srsf3 peaks in the +PDGF-AA condition versus the -PDGF-AA condition within 100 nucleotides upstream of the 5' splice site and within 100 nucleotides downstream of the 3' splice site (Fig. 3E). Additionally, we detected decreased mean coverage in the +PDGF-AA condition within 25 nucleotides downstream of the 5' splice site boundary (Fig. 3E). Taken together, these data show that PDGFRα signaling leads to increased binding of Srsf3 to exons. Finally, we performed unbiased motif enrichment analysis of Srsf3 peaks in unstimulated and PDGF-AA-treated samples, revealing that the mostly highly enriched motifs in -PDGF-AA samples were CACACA and AAGAAG (Fig. 3F; Fig. S5). Of note, these CA-rich

motifs have previously been identified as canonical Srsf3 motifs in a CLIP study utilizing a stably integrated SRSF3-EGFP transgene (Änkö et al., 2012). However, in PDGF-AA-stimulated samples, the most highly enriched motifs were GAAGCG, GAAGAA, and AGAAGA (Fig. 3G; Fig. S5), suggesting that PDGFRα signaling influences Srsf3 binding specificity.

Srsf3 and PDGFRα signaling are associated with differential GC content and length of alternatively-spliced exons

We next probed our RNA-seq dataset to determine whether specific transcript features were associated with Srsf3-dependent AS. When comparing significant AS events between scramble and shSrsf3 samples in the absence of PDGF-AA stimulation, we found that included exons had a significantly higher GC content (median value of 53.4%) than both skipped exons (50.0%) and exons that were not differentially alternatively spliced (51.2%) when Srsf3 is present (Fig. 4A, Table S10). Additionally, we observed that included exons had a significantly lower ratio of downstream intron to exon GC content (0.856) than both skipped exons (0.901) and exons that were not differentially alternatively spliced (0.888) in the presence of Srsf3 (Fig. 4B, Table S10). The same comparisons revealed that the ratio of upstream and downstream intron to exon length was significantly decreased in included exons (median values of 12.4 and 10.6, respectively) as compared to both skipped exons (19.5 and 20.0) and exons that were not differentially alternatively spliced (14.2 and 13.3) in the presence of Srsf3 (Fig. 4C,D, Table S10). Taken together, our data demonstrate that exons which are included in the presence of Srsf3 tend to have a higher GC content and lower intron to exon length ratio.

To determine whether PDGFRα signaling had an effect on the transcript features to which Srsf3 bound, we subsequently examined our eCLIP dataset. We found that the exon GC content was significantly increased in exons bound by Srsf3 in the absence of ligand treatment (median value of 57.9%) as compared to unbound exons (51.5%) (Fig. 4E, Table S10).

However, exon GC content was similar between unbound exons and those bound by Srsf3 upon PDGF-AA stimulation (53.8%) (Fig. 4E, Table S10). These findings indicate that PDGFRα signaling mediates binding of Srsf3 to exons with a lower GC content.

Transcripts bound by Srsf3 that undergo alternative splicing upon PDGFRα signaling encode regulators of PI3K signaling

To determine which transcripts are directly bound by Srsf3 and subject to DE and/or AS, we cross-referenced the eCLIP and RNA-seq datasets. We collated transcripts with an Srsf3 eCLIP peak that were uniquely detected in the -PDGF-AA or +PDGF-AA samples (2,660 transcripts across 3,388 peaks) (Tables S8 and S11). Similarly, we gathered differentially-expressed genes (596) or differentially alternatively-spliced transcripts (985) uniquely found in one of the four treatment comparisons (Fig. 5A, Table S11). Only 32 (5.4%) of the DE genes were directly bound by Srsf3, while 233 (23.7%) of the alternatively-spliced transcripts had an Srsf3 eCLIP peak, with very little overlap (1 transcript) between all three categories (Fig. 5A).

We next sought to identify high-confidence transcripts for which Srsf3 binding had an increased likelihood of contributing to AS. Previous studies revealed enrichment of functional RBP motifs near alternatively-spliced exons (Yee et al., 2019). As such, we correlated the eCLIP peaks with AS events across all four treatment comparisons by identifying transcripts in which Srsf3 bound within an alternatively-spliced exon or within 250 bp of the neighboring introns (Tables S12-S15). In agreement with our findings above for the entire eCLIP dataset, Srsf3 exhibited differential binding in exons and surrounding the 5' and 3' splice sites upon PDGF-AA stimulation in these high-confidence, overlapping datasets (Fig. S6A,B). We performed an unbiased motif enrichment analysis of Srsf3 peaks within the high-confidence, overlapping datasets, again revealing different motifs between ligand treatment conditions and an enrichment of GA-rich motifs in the +PDGF-AA samples (Fig. S6C,D).

To determine whether transcripts that are differentially bound by Srsf3 and undergo differential AS downstream of PDGFRα signaling contribute to shared biological outputs, we conducted GO analysis of the 149 unique transcripts from the high-confidence, overlapping datasets. The most significant terms for biological process involved protein phosphorylation and deacetylation, and RNA metabolism (Fig. 5B). Given that PI3K-mediated PDGFRα signaling is critical for craniofacial development and regulates AS in this context (Dennison et al., 2021; Fantauzzo & Soriano, 2014; Klinghoffer et al., 2002), we turned our focus toward GO terms associated with this signaling pathway. We noted enrichment of PI3K-related GO terms (Fig. 5C), which encompassed the genes *Becn1, Wdr81* and *Acap3* (Fig. 5D). Related to their roles in PI3K signaling, each of these gene products has been shown to regulate membrane and/or endocytic trafficking. Phosphatidylinositol 3-phosphate (PI(3)P) is a critical component of early endosomes and is mainly generated by conversion of phosphatidylinositol (PI) by the class III PI3K complex, which includes Beclin-1 (encoded by *Becn1*) (Wallroth & Haucke, 2018). WDR81 and Beclin-1 have been shown to interact, resulting in decreased endosomal PI(3)P synthesis, PI(3)P turnover and early endosome conversion to late endosomes (Liu et al., 2016). Importantly, this role of WDR81 contributes to RTK degradation (Rapiteanu et al., 2016). Finally, Acap3 is a GTPase-activating protein (GAP) for the small GTPase Arf6, converting Arf6 to an inactive, GDP-bound state (Miura et al., 2016). Arf6 localizes to the plasma membrane and endosomes, and has been shown to regulate endocytic membrane trafficking by increasing PI(4,5)P2 levels at the cell periphery (D'Souza-Schorey and Chavrier, 2006). Further, constitutive activation of Arf6 leads to upregulation of the gene encoding the p85 regulatory subunit of PI3K and increased activity of both PI3K and AKT (Yoo et al., 2019).

Within our data, Srsf3 binding was increased in *Becn1* exon 7 upon PDGF-AA stimulation, at an enriched motif within the high-confidence, overlapping datasets, and we observed a corresponding increase in retention of adjacent intron 7 (Fig. 5D,E). As *Becn1* intron

7 contains a premature termination codon (PTC), this event is predicted to result in nonsense-mediated decay (NMD) in the absence of Srsf3 (Fig. 5E). Srsf3 binding was also increased in *Wdr81* exon 8 in response to PDGF-AA treatment, and our analyses revealed a corresponding increase in excision of adjacent exon 9 (Fig. 5D,E). Because *Wdr81* exon 9 encodes two WD-repeat domains, which are generally believed to form a β propellor structure required for protein interactions (Li & Roberts, 2001), this AS event is predicted to result in a protein missing a functional domain (Fig. 5E). These splicing patterns predict increased levels of Beclin-1 and decreased levels of functional Wdr81 in the presence of Srsf3 and PDGF-AA stimulation, resulting in augmented early endosome formation. Srsf3 binding was additionally increased in *Acap3* exon 19 upon PDGF-AA stimulation, at an enriched motif within the high-confidence, overlapping datasets, and we observed a corresponding increase in excision of adjacent intron 19 (Fig. 5D,E). As *Acap3* intron 19 contains a PTC, this event is predicted to result in more transcripts encoding full-length protein (Fig. 5E).

Finally, as Wdr81 protein levels are predicted to regulate RTK trafficking between early and late endosomes, we confirmed the differential AS of *Wdr81* transcripts between unstimulated scramble cells and scramble cells treated with PDGF-AA ligand for 1 hour by qPCR using primers within constitutively-expressed exons flanking alternatively-spliced exon 9. This analysis revealed a decreased PSI for *Wdr81* in each of three biological replicates upon PDGF-AA ligand treatment (Fig. 5F). Relatedly, we assessed the ratio of larger isoforms of Wdr81 protein (containing the WD3 domain) to smaller isoforms (missing the WD3 domain) via western blotting. Consistent with our RNA-seq and qPCR results, PDGF-AA stimulation for 24 hours in the presence of Srsf3 led to an increase in smaller Wdr81 protein isoforms (Fig. 5G).

Srsf3 regulates early endosome size and phosphorylation of Akt downstream of PDGFRα signaling

Given that Srsf3 differentially binds to transcripts that encode proteins involved in early endosomal trafficking downstream of PDGFRα signaling, we first examined the formation of Rab5-positive early endosomes (Zerial & McBride, 2001) in response to a time course of PDGF-AA ligand stimulation in scramble versus shSrsf3 cells. As expected, Rab5 puncta size increased from 0 min ($9.79 \times 10^{-4} \pm 1.13 \times 10^{-4}$ arbitrary units; mean ± s.e.m.) to 15 min of ligand stimulation ($2.01 \times 10^{-3} \pm 7.20 \times 10^{-4}$ arbitrary units) in scramble cells, and significantly so by 60 min ($2.58 \times 10^{-3} \pm 9.20 \times 10^{-4}$ arbitrary units) (Fig. 6A, C-C"', E-E"', G-G"'). However, this increase was not observed in the absence of Srsf3 ($9.21 \times 10^{-4} \pm 1.61 \times 10^{-4}$ arbitrary units at 60 min) (Fig. 6A, D-D"', F-F"', H-H"'), demonstrating that Srsf3-mediated PDGFRα signaling leads to enlarged early endosomes.

We next examined colocalization of PDGFRα with Rab5, as an estimate of receptor levels in early endosomes. Colocalization levels increased from 0 min (0.332 ± 0.0832 Pearson's correlation coefficient (PCC); mean ± s.e.m.) to 15 min (0.429 ± 0.108 PCC) of PDGF-AA treatment in scramble cells, then decreased to near baseline levels by 60 min (0.348 ± 0.0885 PCC) (Fig. 6B, C-C"', E-E"', G-G"') as a subset of PDGFRα homodimers are likely trafficked to late endosomes (Rogers et al., 2022). Strikingly, shSrsf3 cells exhibited a significant decrease in colocalization between PDGFRα and Rab5 by 60 min of ligand treatment (0.186 ± 0.0102 PCC) (Fig. 6B, D-D"', F-F"', H-H"'), indicating that Srsf3 activity downstream of PDGFRα signaling results in retention of PDGFRα in early endosomes.

Finally, we previously demonstrated that rapid internalization of PDGFRα homodimers following PDGF-AA ligand stimulation is critical for downstream AKT phosphorylation (Rogers et al., 2022). As such, we examined phospho-Akt levels as a readout of PDGFRα activation in early endosomes. While PDGF-AA treatment for 15 min induced a robust phospho-Akt response in scramble cells (13.5 ± 7.39 relative induction, mean ± s.e.m.) this response was muted in shSrsf3 cells at the same timepoint (5.73 ± 1.91) (Fig. 6I). These findings further

suggest that retention of PDGFRα in early endosomes leads to increases in downstream PI3K-mediated Akt signaling. Collectively, our data point to a feedback loop in which PI3K/Akt-mediated PDGFRα signaling results in the nuclear translocation of Srsf3 and the subsequent AS of transcripts to decrease levels of proteins that promote PDGFRα trafficking out of early endosomes (Fig. 6J).

Discussion

In this study, we confirmed our prior *in vivo* results in the mouse embryonic facial mesenchyme (Dennison et al., 2021) that PDGFRα signaling primary regulates gene expression via AS. PDGF-AA-dependent differential gene expression was minimal following one hour of ligand treatment and led to increased expression of immediate early genes *Klf10, Egf3* and *Egr1*, consistent with previous findings (Vasudevan et al., 2015) and in line with the enriched GO terms of regulation of transcription and DNA binding. Alternatively, PDGF-AA-dependent alternatively-spliced transcripts were enriched for protein kinase activity, consistent with our prior AS findings upon disruption of PI3K-mediated PDGFRα signaling in the palatal shelf mesenchyme (Dennison et al., 2021). Importantly, our results demonstrated a significant dependence on the RBP Srsf3 for AS downstream of PDGFRα activation. In fact, we found that 88% of Srsf3-dependent and 99% of PDGF-AA-dependent alternatively-spliced transcripts were responsive to both Srsf3 activity and PDGFRα signaling. As discussed above, Srsf3 is phosphorylated downstream of multiple stimuli (Bavelloni et al., 2014; Dennison et al., 2021; Fantauzzo & Soriano, 2014; Long et al., 2019; Zhou et al., 2012), and it is likely that these additional inputs contributed to Srsf3-dependent AS that was non-responsive to PDGF-AA treatment. Further, our previous mass spectrometry screen identified 11 additional RBPs involved in AS that are phosphorylated by Akt downstream of PI3K-mediated PDGFRα signaling in primary MEPM cells (Fantauzzo & Soriano, 2014), which may account for the small fraction of

PDGF-AA-dependent AS that was non-responsive to Srsf3 knockdown. However, our RNA-seq results together with the phenotypic overlap of embryos with neural crest-specific ablation of *Srsf3* and mutant mouse models of *Pdgfra* and/or its ligands (Andrae et al., 2016; Dennison et al., 2021; Ding et al., 2004; Fantauzzo & Soriano, 2014; Fredriksson et al., 2012; Klinghoffer et al., 2002; Soriano, 1997) make a compelling case for Srsf3 serving as a critical effector of PDGFRα signaling in the facial mesenchyme.

Here, we observed that Srsf3-dependent skipped exon events were enriched for transcripts with a +ΔPSI (exon skipped more often in shSrsf3 samples) in the absence of PDGF-AA stimulation, consistent with Srsf3 promoting exon inclusion. Alternatively, PDGF-AA ligand treatment led to an increase in the percentage of Srsf3-dependent transcripts with a -ΔPSI (exon included more often in shSrsf3 samples), suggesting that PDGFRα signaling causes decreased exon inclusion in the presence of Srsf3. Interestingly, a recent paper found that tethering Srsf3 downstream of the 5' splice site or upstream of the 3' splice site using MS2 stem loops did not lead to AS of a splicing reporter (Schmok et al., 2024). However, the assay did not test tethering within the exon and used a single minigene sequence context, and thus had the potential to lead to false negative results (Schmok et al., 2024). Whether phosphorylation of Srsf3 directly influences its binding to target RNAs or acts to modulate Srsf3 protein-protein interactions which then contribute to differential RNA binding remains to be determined, though findings from Schmok et al., 2024 may argue for the latter mechanism. Studies identifying proteins that differentially interact with Srsf3 in response to PDGF-AA ligand stimulation are ongoing and will shed light on these mechanisms.

This study represents the first endogenous CLIP analysis of Srsf3 in the absence of protein tagging, and thus circumvents potential limitations with prior approaches in which assayed RBPs were overexpressed and/or fused to another protein. Our eCLIP analyses revealed several changes in Srsf3 transcript binding downstream of PDGF-AA stimulation,

including increased Srsf3 binding to exons and loss of Srsf3 binding to canonical CA-rich motifs. A previous CLIP study using a stably integrated SRSF3-EGFP transgene in mouse P19 cells determined that SRSF3 binding was enriched in exons, particularly within 100 nucleotides of the 5' and, to a lesser extent, 3' splice sites (Änkö et al., 2012), consistent with our results. This same study identified a CA-rich canonical SRSF3 motif (Änkö et al., 2012). While such motifs were identified here in the absence of PDGF-AA treatment, they were lost upon ligand stimulation. Again, this shift could be due to loss of RNA binding owing to electrostatic repulsion and/or changes in ribonucleoprotein composition and will be the subject of future studies.

Our findings additionally pointed to novel properties of exons whose inclusion is dependent on Srsf3 in the absence of PDGFRα signaling. We demonstrated that these included exons had a higher GC content, a lower ratio of downstream intron to exon GC content and a decreased ratio of upstream and downstream intron to exon length. These findings are consistent with previous results demonstrating that included exons tend to have higher GC content than the flanking introns (Amit et al., 2012). Of note, PDGF-AA ligand stimulation resulted in binding of Srsf3 to exons with a lower GC content, again suggesting that phosphorylation of the RBP downstream of this signaling axis promotes exon skipping.

By cross-referencing our RNA-seq and eCLIP datasets, we showed that 24% of the alternatively-spliced transcripts across our four treatment comparisons had an Srsf3 eCLIP peak. As Srsf3 also has functions in the cytoplasm, such as RNA trafficking, translation and degradation (Howard & Sanford, 2015), the additional eCLIP peaks may reflect alternate roles for Srsf3 in RNA metabolism. Conversely, Srsf3-mediated AS may be delayed following transcript binding in the short timeframe of our experimental design. However, the extent of overlap that we observed is in line with previous studies correlating alternatively-spliced transcripts upon knockdown of an RBP with endogenous eCLIP results for that same RBP, including Rbfox2 (10%) (Moss et al., 2023) and LUC7L2 (18-26%) (Jourdain et al., 2021). The

445 degree to which our RNA-seq and eCLIP datasets overlapped here points to the robustness and
446 biological significance of our findings.

447 Our combined analyses demonstrated that Srsf3 binds and mediates the AS of
448 transcripts that encode proteins that regulate PI3K signaling and early endosomal trafficking
449 downstream of PDGFRα activation, including *Becn1, Wdr81* and *Acap3.* Homozygous missense
450 mutations in *WDR81* cause Cerebellar ataxia, impaired intellectual development, and
451 dysequilibrium syndrome 2 (OMIM 610185) in humans (Gulsuner et al., 2011), with some
452 patients exhibiting coarse facial features and strabismus (Garcias & Roth, 2007), pointing to a
453 critical role for this gene product in craniofacial development. Consistently, we found that related
454 GO terms, such as phosphatidylinositol phosphate binding and endosome to lysosome
455 transport, were significantly enriched among alternatively-spliced transcripts in murine
456 embryonic facial mesenchyme upon loss of PI3K binding to PDGFRα and/or knockdown of
457 *Srsf3* (Dennison et al., 2021). These data further confirm that our iMEPM model system served
458 as a powerful platform to uncover mechanisms that are utilized during craniofacial development
459 *in vivo*.

460 Our subsequent *in vitro* validation studies showed that Srsf3-mediated PDGFRα
461 signaling results in enlarged early endosomes, retention of the receptor in these early
462 endosomes and increased downstream PI3K-mediated Akt signaling. Relatedly, we and others
463 have linked spatial organization with the propagation of PDGFRα signaling, such that rapid
464 internalization of the receptors into early endosomes or autophagy of the receptors are required
465 for maximal phosphorylation of AKT downstream of PDGFRα activation (Rogers et al., 2022;
466 Simpson et al., 2024). Together, these results indicate a feedback loop at play in the
467 craniofacial mesenchyme in which stimulation of PDGFRα homodimer signaling leads to Srsf3-
468 dependent AS of transcripts, a subsequent increase in the levels of proteins that maintain the
469 receptor in early endosomes and a corresponding decrease in the levels of proteins that

promote trafficking of the receptor to late endosomes for eventual degradation. These findings thus represent a novel mechanism by which PDGFRα activity is maintained and propagated within the cell. Whether similar mechanisms exist downstream of alternate RTKs or contribute to increases in the phosphorylation of effector proteins other than Akt remain to be determined. In the future, it will be worthwhile to attempt to functionally link the AS of transcripts such as *Becn1, Wdr81* and/or *Acap3* to the endosomal trafficking changes observed above using splice-switching antisense oligonucleotides (ASOs).

Taken together, our findings significantly enhance our understanding of the molecular mechanisms by which Srsf3 activity is regulated downstream of growth factor stimulation. Interestingly, a recent study demonstrated that retention of another shuttling SR protein, Srsf1, exclusively in the nucleus resulted in widespread ciliary defects in mice (Haward et al., 2021). This finding indicates that dissecting nuclear from cytoplasmic functions of SR proteins can provide powerful insight into the physiological relevance of each. Going forward, it will be critical to explore the *in vivo* consequences of abrogating Akt-mediated phosphorylation of Srsf3 and comparing the resulting phenotype to those of embryos with constitutive or conditional ablation of *Srsf3* in the neural crest lineage (Dennison et al., 2021; Jumaa et al., 1999). These experiments are ongoing and should shed considerable light on the roles of RBP post-translational modifications during development.

Materials and Methods

Generation of scramble and Srsf3 *shRNA iMEPM cell lines*

Immortalized mouse embryonic palatal mesenchyme (iMEPM) cells were derived from a male *Cdkn2a*$^{-/-}$ embryo as previously described (Fantauzzo & Soriano, 2017). iMEPM cells were cultured in growth medium [Dulbecco's modified Eagle's medium (Gibco, Thermo Fisher Scientific, Waltham, MA, USA) supplemented with 50 U/mL penicillin (Gibco), 50 μg/mL

streptomycin (Gibco) and 2 mM L-glutamine (Gibco) containing 10% fetal bovine serum (FBS) (Hyclone Laboratories Inc., Logan, UT, USA)] and grown at 37°C in 5% carbon dioxide. iMEPM cells were tested for mycoplasma contamination using the MycoAlert Mycoplasma Detection Kit (Lonza Group Ltd, Basel, Switzerland). Packaged lentiviruses containing pLV[shRNA]-EGFP:T2A:Puro-U6>Scramble_shRNA (vectorID: VB010000-0009mxc) with sequence CCTAAGGTTAAGTCGCCCTCGCTCGAGCGAGGGCGACTTAACCTTAGG or pLV[shRNA]-EGFP:T2A:Puro-U6>mSrsf3[shRNA#1] (vectorID: VB900060-7699yyh) with sequence GAATGATAAAGCGGTGTTTACTCGAGTAAACACCGCTTTATCATTCC were purchased from VectorBuilder (Chicago, IL, USA). Medium containing lentivirus for a multiplicity of infection of 10 for 200,000 cells with the addition of 10 ug/mL polybrene was added to iMEPM cells for 16 h, and cells were subsequently grown in the presence of 4 ug/mL puromycin for 10 days. Cells with the highest GFP expression (top 20%) were isolated on a Moflo XDP 100 cell sorter (Beckman Coulter Inc., Brea, CA, USA) and expanded. Srsf3 expression in scramble and *Srsf3* shRNA cell lines was confirmed by western blotting. Once the stable cell lines were established, they were split at a ratio of 1:4 for maintenance. Scramble and *Srsf3* shRNA cells were used for experiments at passages 9-20.

Immunoprecipitation and western blotting

To induce PDGFRα signaling, cells at ~70% confluence were serum starved for 24 h in starvation medium [Dulbecco's modified Eagle's medium (Gibco) supplemented with 50 U/mL penicillin (Gibco), 50 μg/mL streptomycin (Gibco) and 2 mM L-glutamine (Gibco) containing 0.1% FBS (Hyclone Laboratories Inc.)] and stimulated with 10 ng/mL rat PDGF-AA ligand (R&D Systems, Minneapolis, MN, USA) diluted from a 1.5 μg/mL working solution in 40 nM HCl containing 0.1% BSA for the indicated length of time. When applicable, UV-crosslinking was performed at 254 nm and 400 mJ/cm^2 using a Vari-X-Link system (UVO3 Ltd, Cambridgeshire,

UK). For immunoprecipitation of Srsf3, cells were resuspended in ice-cold CLIP lysis buffer [50 mM Tris-HCl pH 7.4, 100 mM NaCl, 1% NP-40, 0.1% SDS, 0.5% sodium deoxycholate, 1x complete Mini protease inhibitor cocktail (Roche, MilliporeSigma, Burlington, MA, USA), 1 mM PMSF, 10 mM NaF, 1 mM Na_3VO_4, 25 mM β-glycerophosphate]. Cleared lysates were collected by centrifugation at 18,000 *g* for 20 min at 4°C. Anti-Srsf3 antibody (10 μg/sample) (ab73891, Abcam, Waltham, MA, USA) was added to protein A Dynabeads (125 μL/sample) (Thermo Fisher Scientific) washed twice in ice-cold CLIP lysis buffer and incubated for 45 min at room temperature. Cells lysates were incubated with antibody-conjugated Dynabeads or Dynabeads M-280 sheep anti-rabbit IgG (Thermo Fisher Scientific) washed twice in ice-cold CLIP lysis buffer overnight at 4°C. The following day, Dynabeads were washed twice each with ice-cold high salt wash buffer [50 mM Tris-HCl pH 7.4, 1M NaCl, 1 mM EDTA, 1% NP-40, 0.1% SDS, 0.5% sodium deoxycholate] followed by ice-cold wash buffer [20 mM Tris-HCl pH 7.4, 10 mM $MgCl_2$, 0.2% Tween-20]. The precipitated proteins were eluted with 1x NuPAGE LDS buffer (Thermo Fisher Scientific) containing 100 mM dithiothreitol, heated for 10 minutes at 70°C, and separated by SDS-PAGE. For western blotting of whole-cell lysates, protein lysates were generated by resuspending cells in ice-cold NP-40 lysis buffer (20 mM Tris-HCl pH 8, 150 mM NaCl, 10% glycerol, 1% Nonidet P-40, 2 mM EDTA, 1x complete Mini protease inhibitor cocktail (Roche), 1 mM PMSM, 10 mM NaF, 1 mM Na_3VO_4, 25 mM β-glycerophosphate) and collecting cleared lysates by centrifugation at 13,400 *g* at 4°C for 20 min. Laemmli buffer containing 10% β-mercaptoethanol was added to the lysates, which were heated for 5 min at 100°C. Proteins were subsequently separated by SDS-PAGE. Western blot analysis was performed according to standard protocols using horseradish peroxidase-conjugated secondary antibodies. Blots were imaged using a ChemiDoc XRS+ (Bio-Rad Laboratories, Inc., Hercules, CA, USA) or a ChemiDoc (Bio-Rad Laboratories, Inc.). The following primary antibodies were used for western blotting: Srsf3 (1:1,000, ab73891, Abcam), Gapdh (1:50,000, 60004, Proteintech Group, Inc.,

Rosemont, IL, USA), Wdr81 (1:1,000, 24874-1-AP, Proteintech Group, Inc.), phospho-Akt (Ser473) (1:1,000, 9271, Cell Signaling Technology, Inc., Danvers, MA, USA), Akt (1:1,000, 9272, Cell Signaling Technology, Inc.), horseradish peroxidase-conjugated goat anti-mouse IgG (1:20,000, 115035003, Jackson ImmunoResearch Inc., West Grove, PA, USA), horseradish peroxidase-conjugated goat anti-rabbit IgG (1:20,000, 111035003;, Jackson ImmunoResearch Inc.). Quantifications of signal intensity were performed with ImageJ software (version 1.53t, National Institutes of Health, Bethesda, MD, USA). The relative ratio of Wdr81 isoforms was calculated as the fraction of the larger isoform divided by the fraction of the smaller isoform following normalization to Gapdh levels. Relative phospho-Akt levels were determined by normalizing to total Akt levels. When applicable, statistical analyses were performed with Prism 10 (GraphPad Software Inc., San Diego, CA, USA) using a two-tailed, ratio paired *t*-test within each cell line and a two-tailed, unpaired *t*-test with Welch's correction between each cell line. Immunoprecipitation and western blotting experiments were performed across three independent experiments.

RNA-sequencing and related bioinformatics analyses

8 x 10^5 cells obtained from each of three independent biological replicates per treatment were frozen on liquid nitrogen and stored at -80°C. Following thawing, total RNA was simultaneously isolated from all samples using the RNeasy Mini Kit (Qiagen, Inc., Germantown, MD, USA) according to the manufacturer's instructions. RNA was forwarded to the University of Colorado Cancer Center Genomics Shared Resource for quality control, library preparation, and sequencing. RNA purity, quantity and integrity were assessed with a NanoDrop (Thermo Fisher Scientific) and a 4200 TapeStation System (Agilent Technologies, Inc., Santa Clara, CA, USA) prior to library preparation. Total RNA (200 ng) was used for input into the Universal Plus mRNA-Seq kit with NuQuant (Tecan Group Ltd., Männedorf, Switzerland). Dual index, stranded

libraries were prepared and sequenced on a NovaSeq 6000 Sequencing System (Illumina, San Diego, CA, USA) to an average depth of ~54 million read pairs (2x150 bp reads).

Raw sequencing reads were de-multiplexed using bcl2fastq (Illumina). Trimming, filtering and adapter contamination removal was performed using BBDuk (from the BBmap v35.85 tool suite) (Bushnell, 2015). For differential expression analysis, transcript abundance was quantified using Salmon (v1.4.0) (Patro et al., 2017) and a decoy-aware transcriptome index prepared using GENCODE (Frankish et al., 2019) GRCm39 M26. Gene level summaries were calculated using tximport (Soneson et al., 2016) in R and differential expression was measured using DESeq2 (v.1.32.0) (Love et al., 2014). Significant changes in gene-level expression are reported for cases with adjusted $P \leq 0.05$ and fold change $|FC| \geq 2$. Spearman correlation was computed between conditions for differentially-expressed genes. For alternative splicing analysis, raw FASTQ were trimmed to a uniform length of 125 bp. Reads were aligned to the mouse genome (GRCm39 Gencode M26) using STAR (v.2.7.9a) (Dobin et al., 2013). Additional parameters for STAR: --outFilterType BySJout --outFilterMismatchNmax 10 --outFilterMismatchNoverLmax 0.04 --alignEndsType EndToEnd --runThreadN 16 --alignSJDBoverhangMin 4 --alignIntronMax 300000 --alignSJoverhangMin 8 --alignIntronMin 20. All splice junctions detected in at least 1 read from the first pass alignment were used in a second pass alignment, per software documentation. Alternative splicing events were detected using rMATS (v4.0.2, default parameters plus '—cstat 0.0001') (Shen et al. 2014). Reads mapping to the splice junction as well as those mapping to the exon body were used in downstream analyses. Detected events were compared between treatment groups and considered significant with false discovery rate (FDR) ≤ 0.05, a difference in percent spliced in ($|\Delta PSI|$) ≥ 0.05 and event detection in at least 10 reads in either condition. Raw read pairs, trimmed read pairs for Salmon input, Salmon mapping rate per sample, trimmed read pairs (125 bp) for STAR input and STAR unique mapping rate can be found in Table S1. Gene ontology

595 analysis was performed with various libraries from the Enrichr gene list enrichment analysis tool
596 (Chen et al., 2013; Kuleshov et al., 2016) and terms with $P < 0.05$ were considered significant.
597
598 *qPCR*
599 Total RNA was isolated using the RNeasy mini kit (Qiagen, Germantown, MD, USA)
600 according to the manufacturer's instructions. First-strand cDNA was synthesized using a ratio of
601 2:1 random primers:oligo (dT) primer and SuperScript II RT (Invitrogen, Thermo Fisher
602 Scientific) according to the manufacturer's instructions. All reactions were performed with 1×
603 ThermoPol buffer [0.02 M Tris (pH 8.8), 0.01 M KCl, 0.01 M $(NH_4)_2SO_4$, 2 mM $MgSO_4$ and 0.1%
604 Triton X-100], 200 µM dNTPs, 200 nM primers (Integrated DNA Technologies, Inc., Coralville,
605 IA, USA), 0.6 U Taq polymerase and 1 µg cDNA in a 25 µL reaction volume. The primers used
606 can be found in Table S16. The following PCR protocol was used for *Arhgap12*: step1, 3 min at
607 94°C; step 2, 30 s at 94°C; step 3, 30 s at 47°C; step 4, 30 s at 72°C; repeat steps 2-4 for 34
608 cycles; and step 5, 5 min at 72°C. The following PCR protocol was used for *Cep55*: step1, 3 min
609 at 94°C; step 2, 30 s at 94°C; step 3, 30 s at 48°C; step 4, 30 s at 72°C; repeat steps 2-4 for 34
610 cycles; and step 5, 5 min at 72°C. Two-thirds of total PCR products were electrophoresed on a
611 2% agarose/TBE gel containing ethidium bromide and photographed on an Aplegen Omega
612 Fluor Gel Documentation System (Aplegen Inc., Pleasanton, CA, USA). Quantifications of band
613 intensity were performed with ImageJ software (version 1.53t, National Institutes of Health). The
614 following PCR protocol was used for *Wdr81*: step1, 3 min at 94°C; step 2, 30 s at 94°C; step 3,
615 30 s at 50°C; step 4, 30 s at 72°C; repeat steps 2-4 for 24 cycles; and step 5, 2 min at 72°C.
616 PCR products were purified with AMPure XP Reagent (Beckman Coulter, Brea, CA, USA) and
617 analyzed on a 4150 TapeStation System (Agilent Technologies, Inc.) using High Sensitivity
618 D1000 ScreenTape (Agilent Technologies, Inc.). The PSI was calculated independently for each
619 sample as the percentage of the larger isoform divided by the total abundance of all isoforms
620 within the given gel lane or TapeStation sample. Statistical analyses were performed with Prism

10 (GraphPad Software) using a two-tailed, unpaired *t*-test with Welch's correction. qPCR reactions were performed using three biological replicates.

Enhanced UV-crosslinking and immunoprecipitation and related bioinformatics analyses

Experiments were performed as previously described in biological duplicates (Van Nostrand et al., 2016, 2017). Briefly, 2 million cells per treatment were serum starved and treated with 10 ng/mL PDGF-AA as described above. Cells were subsequently UV-crosslinked at 254 nm and 400 mJ/cm^2, scraped in 1x phosphate buffered saline (PBS) and transferred to 1.5 mL Eppendorf tubes, at which point excess PBS was removed and cells were frozen on liquid nitrogen and stored at -80°C. Following thawing, cells were lysed in ice-cold CLIP lysis buffer, sonicated by BioRuptor (Diagenode, Denville, NJ, USA) and treated with RNase I (Thermo Fisher Scientific). 2% of lysates were set aside as size-matched input samples. Srsf3-RNA complexes were immunoprecipitated with anti-Srsf3 antibody (10 μg per sample) (ab73891, Abcam) conjugated to protein A Dynabeads (Thermo Fisher Scientific). IP samples were washed and dephosphorylated with FastAP (New England Biolabs, Ipswich, MA, USA) and T4 PNK (New England Biolabs). IP samples underwent on-bead ligation of barcoded RNA adapters (/5phos/rArGrArUrCrGrGrArArGrArGrCrGrUrCrGrUrG/3SpC3/) to the 3' end using T4 RNA ligase (New England Biolabs). Following elution, protein-RNA complexes were run on 4-12% Bis-Tris 1.5 mm gels (Thermo Fisher Scientific) and transferred onto nitrocellulose membranes. The 20-75 kDa region was excised and digested with proteinase K (New England Biolabs). RNA was isolated with acid phenol/chloroform/isoamyl alcohol (pH 6.5) (Thermo Fisher Scientific), reverse transcribed with Superscript III (Thermo Fisher Scientific) and treated with ExoSAP-IT (Affymetrix, Thermo Fisher Scientific) to remove excess primers and unincorporated nucleotides. Samples underwent 3' ligation of barcoded DNA adapters (/5Phos/NNNNNNNNNNAGATCGGAAGAGCACACGTCTG/3SpC3/), clean-up with Dynabeads MyOne Silane (Thermo Fisher Scientific) and qPCR to determine the appropriate number of

PCR cycles. Libraries were then amplified with Q5 PCR mix (New England Biolabs) for a total of 16-25 cycles. Libraries were forwarded to the University of Colorado Cancer Center Genomics Shared Resource for quality control and sequencing. Sample integrity was assessed with a D1000 ScreenTape System (Agilent Technologies, Inc.) and sequenced on a NovaSeq 6000 Sequencing System (Illumina) to an average depth of ~20 million read pairs (2x150 bp reads).

Raw sequencing reads were de-multiplexed using bcl2fastq (Illumina). Adapters were trimmed using cutadapt (v.1.18) (Martin, 2011). Trimmed reads were quality filtered and collapsed using a combination of FASTX-Toolkit (v.0.0.14) (http://hannonlab.cshl.edu/fastx_toolkit), seqtk (v.1.3-r106) (https://github.com/lh3/seqtk) and custom scripts. After collapsing the reads, unique molecular identifiers were removed using seqtk. STAR index for repetitive elements was created using repetitive sequences from msRepDB (Liao et al., 2022). Reads ≥ 18 nt were mapped to the repetitive elements using STAR (v.2.7.9a) (Dobin et al. 2013). Reads unmapped to the repetitive elements were mapped to the mouse genome (GRCm39 Gencode M26) using STAR (v.2.7.9a) with parameters alignEndsType: EndtoEnd and outFilterMismatchNoverReadLmax: 0.04. Peaks were called using omniCLIP (v.0.20) (Drewe-Boss et al., 2018) with the foreground penalty (--fg_pen) parameter set to 5. Peaks were annotated and motif analyses performed using RCAS (v.1.19.0) (Uyar et al., 2017) and custom R script. Motif enrichment significance was calculated using a *t*-test. For visualization purposes, bigWig files were created from bam files using deepTools (v.3.5.5) (Ramírez et al., 2016). Peaks were visualized in Integrative Genomics Viewer (v.2.13.0) (Robinson et al., 2011). Intron and exon features were calculated using Matt (v.1.3.1) (Gohr & Irimia, 2019), and statistical analyses were performed using a Mann-Whitney U test. For overlap of eCLIP peaks and alternative splicing events, peak coordinates were taken from omniCLIP bed files and alternative splicing coordinates were taken from rMATS output. Overlapping coordinates from alternative splicing events were defined following the rMAPS default values (Park et al., 2016). Overlap was calculated using valr (v.0.6.4) (Riemondy et al.,

673 2017) and custom R scripts. Raw read pairs, trimmed read pairs, collapsed reads, reads after
674 removing repetitive elements, mapped reads, peaks and annotated peaks can be found in Table
675 S7. Gene ontology analysis was performed with various libraries from the Enrichr gene list
676 enrichment analysis tool (Chen et al., 2013; Kuleshov et al., 2016) and terms with $P < 0.05$ were
677 considered significant.
678
679 *Immunofluorescence analysis*
680 Cells were seeded onto glass coverslips at ~40% confluency per 24-well plate well in
681 iMEPM growth medium. After 24 h, cells were serum starved and treated with 10 ng/mL PDGF-
682 AA as described above. Cells were fixed in 4% paraformaldehyde (PFA) in PBS with 0.1%
683 Triton X-100 for 10 min and washed in PBS. Cells were blocked for 1 h in 5% normal donkey
684 serum (Jackson ImmunoResearch Inc.) in PBS and incubated overnight at 4°C in primary
685 antibody diluted in 1% normal donkey serum in PBS. After washing in PBS, cells were
686 incubated in Alexa Fluor 488-conjugated donkey anti-rabbit secondary antibody (1:1,000;
687 A21206; Invitrogen) or Alexa Fluor 546-conjugated donkey anti-mouse secondary antibody
688 (1:1,000; A10036; Invitrogen) diluted in 1% normal donkey serum in PBS with 2 µg/ml DAPI
689 (Sigma-Aldrich, St. Louis, MO, USA) for 1 h. Cells were mounted in VECTASHIELD HardSet
690 Antifade Mounting Medium (Vector Laboratories, Inc., Burlingame, CA, USA) and photographed
691 using an Axiocam 506 mono digital camera (Carl Zeiss Microscopy LLC, White Plains, NY,
692 USA) fitted onto an Axio Observer 7 fluorescence microscope (Carl Zeiss Microscopy LLC) with
693 the 63x oil objective with a numerical aperture of 1.4 at room temperature. The following
694 antibodies were used for immunofluorescence analysis: Rab5 (1:200, C8B1, 3547, Cell
695 Signaling Technology Inc.), PDGFRα (1:20, AF1062, R&D Systems). For assessment of Rab5
696 puncta size and colocalization experiments, three independent trials, or biological replicates,
697 were performed. For each biological replicate, 20 technical replicates consisting of individual
698 cells were imaged with Z-stacks (0.24 µm between Z-stacks with a range of 1–6 Z-stacks) per

timepoint. Images were deconvoluted using ZEN Blue software (Carl Zeiss Microscopy LLC) using the 'Better, fast (Regularized Inverse Filter)' setting. Extended depth of focus was applied to Z-stacks using ZEN Blue software (Carl Zeiss Microscopy LLC) to generate images with the maximum depth of field. For assessment of Rab5 puncta size, images were converted to 8-bit using Fiji software (version 2.14.0/1.54f). Images were subsequently converted to a mask and watershed separation was applied. A region of interest (ROI) was drawn around each Rab5-positive cell and particles were analyzed per cell using the "analyze particles" function. For colocalization measurements, an ROI was drawn around each PDGFRα-positive cell in the corresponding Cy3 (marker) channel using Fiji. For each image with a given ROI, the Cy3 channel and the EGFP channel were converted to 8-bit images. Colocalization was measured using the Colocalization Threshold function, where the rcoloc value [Pearson's correlation coefficient (PCC)] was used in statistical analysis. Statistical analyses were performed on the average values from each biological replicate with Prism 10 (GraphPad Software Inc.) using a two-way ANOVA followed by uncorrected Fisher's LSD test.

Acknowledgements

We are grateful to Jessica Johnston and Erin Binne for technical assistance, and Drs. Allison Swain, Justin Roberts and Aaron Johnson at the University of Colorado Anschutz Medical Campus for advice on eCLIP experiments. Cell sorting was performed at the University of Colorado Cancer Center Flow Cytometry Shared Resource with assistance from Dr. Dmitry Baturin. RNA-seq and eCLIP sequencing experiments were performed at the University of Colorado Cancer Center Genomics Shared Resource. We thank members of the Fantauzzo laboratory for their critical comments on the manuscript.

Competing Interests

724 The authors declare no competing or financial interests.

725

726 **Author contributions**

727 Conceptualization: TEF, MS, NM, KAF; Methodology: TEF, MS, NM, KAF; Formal analysis:
728 TEF, MS, EDL, KAF; Investigation: TEF, MS, EDL; Writing – Original Draft: TEF, KAF; Writing –
729 Review & Editing: MS, EDL, NM; Visualization: TEF, MS, KAF; Supervision: NM, KAF; Project
730 administration: KAF; Funding acquisition: TEF, KAF.

731

732 **Funding**

733 This work was supported by National Institutes of Health grants R01DE030864 (to K.A.F.),
734 R35GM147025 (to N.M.), the University of Colorado Anschutz Medical Campus RNA
735 Bioscience Initiative (to N.M. and M.P.S.) and F31DE032252 (to T.E.F.). The Flow Cytometry
736 Shared Resource and Genomics Shared Resource are supported by National Institutes of
737 Health grant P30CA046934.

738

739 **Data Availability**

740 The eCLIP and RNA-sequencing datasets generated during this study have been deposited in
741 GEO under SuperSeries accession number GSE263170. Custom analysis scripts will be
742 provided by Dr. Larson through GitHub.

743

744 **References**

745 Akerman, M., David-Eden, H., Pinter, R. Y., & Mandel-Gutfreund, Y. (2009). A computational
746 approach for genome-wide mapping of splicing factor binding sites. *Genome Biology*,
747 *10*(3), R30. https://doi.org/10.1186/gb-2009-10-3-r30
748 Amit, M., Donyo, M., Hollander, D., Goren, A., Kim, E., Gelfman, S., Lev-Maor, G., Burstein, D.,
749 Schwartz, S., Postolsky, B., Pupko, T., & Ast, G. (2012). Differential GC Content

between Exons and Introns Establishes Distinct Strategies of Splice-Site Recognition. *Cell Reports*, *1*(5), 543–556. https://doi.org/10.1016/j.celrep.2012.03.013

Andrae, J., Gouveia, L., Gallini, R., He, L., Fredriksson, L., Nilsson, I., Johansson, B. R., Eriksson, U., & Betsholtz, C. (2016). A role for PDGF-C/PDGFRα signaling in the formation of the meningeal basement membranes surrounding the cerebral cortex. *Biology Open*, *5*(4), 461–474. https://doi.org/10.1242/bio.017368

Änkö, M.-L., Müller-McNicoll, M., Brandl, H., Curk, T., Gorup, C., Henry, I., Ule, J., & Neugebauer, K. M. (2012). The RNA-binding landscapes of two SR proteins reveal unique functions and binding to diverse RNA classes. *Genome Biology*, *13*(3), R17. https://doi.org/10.1186/gb-2012-13-3-r17

Bavelloni, A., Piazzi, M., Faenza, I., Raffini, M., D'Angelo, A., Cattini, L., Cocco, L., & Blalock, W. L. (2014). Prohibitin 2 represents a novel nuclear AKT substrate during all- *trans* retinoic acid–induced differentiation of acute promyelocytic leukemia cells. *The FASEB Journal*, *28*(5), 2009–2019. https://doi.org/10.1096/fj.13-244368

Bebee, T. W., Park, J. W., Sheridan, K. I., Warzecha, C. C., Cieply, B. W., Rohacek, A. M., Xing, Y., & Carstens, R. P. (2015). The splicing regulators Esrp1 and Esrp2 direct an epithelial splicing program essential for mammalian development. *eLife*, *4*, e08954. https://doi.org/10.7554/eLife.08954

Bushnell, B. (2015). *BBMap*. Https://Sourceforge.Net/Projects/Bbmap/. https://sourceforge.net/projects/bbmap/

Chen, E. Y., Tan, C. M., Kou, Y., Duan, Q., Wang, Z., Meirelles, G. V., Clark, N. R., & Ma'ayan, A. (2013). Enrichr: Interactive and collaborative HTML5 gene list enrichment analysis tool. *BMC Bioinformatics*, *14*, 128. https://doi.org/10.1186/1471-2105-14-128

Choi, S. J., Marazita, M. L., Hart, P. S., Sulima, P. P., Field, L. L., McHenry, T. G., Govil, M., Cooper, M. E., Letra, A., Menezes, R., Narayanan, S., Mansilla, M. A., Granjeiro, J. M., Vieira, A. R., Lidral, A. C., Murray, J. C., & Hart, T. C. (2009). The PDGF-C regulatory

region SNP rs28999109 decreases promoter transcriptional activity and is associated with CL/P. *European Journal of Human Genetics*, *17*(6), 774–784. https://doi.org/10.1038/ejhg.2008.245

Cibi, D. M., Mia, M. M., Guna Shekeran, S., Yun, L. S., Sandireddy, R., Gupta, P., Hota, M., Sun, L., Ghosh, S., & Singh, M. K. (2019). Neural crest-specific deletion of Rbfox2 in mice leads to craniofacial abnormalities including cleft palate. *eLife*, *8*, e45418. https://doi.org/10.7554/eLife.45418

D'Souza-Schorey, C., & Chavrier, P. (2006). ARF proteins: roles in membrane traffic and beyond. *Nature Reviews Molecular Cell Biology*, *7*(5), 347-358. https://doi.org/10.1038/nrm1910

Dennison, B. J. C., Larson, E. D., Fu, R., Mo, J., & Fantauzzo, K. A. (2021). Srsf3 mediates alternative RNA splicing downstream of PDGFRα signaling in the facial mesenchyme. *Development*, *148*(14), dev199448. https://doi.org/10.1242/dev.199448

Ding, H., Wu, X., Boström, H., Kim, I., Wong, N., Tsoi, B., O'Rourke, M., Koh, G. Y., Soriano, P., Betsholtz, C., Hart, T. C., Marazita, M. L., Field, L. L., Tam, P. P. L., & Nagy, A. (2004). A specific requirement for PDGF-C in palate formation and PDGFR-α signaling. *Nature Genetics*, *36*(10), 1111–1116. https://doi.org/10.1038/ng1415

Dobin, A., Davis, C. A., Schlesinger, F., Drenkow, J., Zaleski, C., Jha, S., Batut, P., Chaisson, M., & Gingeras, T. R. (2013). STAR: ultrafast universal RNA-seq aligner. *Bioinformatics, 29*(1), 15-21. https://doi.org/10.1093/bioinformatics/bts635

Drewe-Boss, P., Wessels, H.-H., & Ohler, U. (2018). omniCLIP: Probabilistic identification of protein-RNA interactions from CLIP-seq data. *Genome Biology*, *19*(1), 183. https://doi.org/10.1186/s13059-018-1521-2

799 Fantauzzo, K. A., & Soriano, P. (2014). PI3K-mediated PDGFR signaling regulates survival and
800 proliferation in skeletal development through p53-dependent intracellular pathways.
801 *Genes & Development*, *28*(9), 1005–1017. https://doi.org/10.1101/gad.238709.114
802 Fantauzzo, K. A., & Soriano, P. (2017). Generation of an immortalized mouse embryonic palatal
803 mesenchyme cell line. *PLOS ONE*, *12*(6), e0179078.
804 https://doi.org/10.1371/journal.pone.0179078
805 Forman, T. E., Dennison, B. J. C., & Fantauzzo, K. A. (2021). The Role of RNA-Binding Proteins
806 in Vertebrate Neural Crest and Craniofacial Development. *Journal of Developmental*
807 *Biology*, *9*(3), 34. https://doi.org/10.3390/jdb9030034
808 Frankish, A., Diekhans, M., Ferreira, A. M., Johnson, R., Jungreis, I., Loveland, J., Mudge, J.
809 M., Sisu, C., Wright, J., Armstrong, J., Barnes, I., Berry, A., Bignell, A., Carbonell Sala,
810 S., Chrast, J., Cunningham, F., Di Domenico, T., Donaldson, S., Fiddes, I. T., … Flicek,
811 P. (2019). GENCODE reference annotation for the human and mouse genomes. *Nucleic*
812 *Acids Research*, *47*(D1), D766-763. https://doi.org/10.1093/nar/gky955
813 Fredriksson, L., Nilsson, I., Su, E. J., Andrae, J., Ding, H., Betsholtz, C., Eriksson, U., &
814 Lawrence, D. A. (2012). Platelet-Derived Growth Factor C Deficiency in C57BL/6 Mice
815 Leads to Abnormal Cerebral Vascularization, Loss of Neuroependymal Integrity, and
816 Ventricular Abnormalities. *The American Journal of Pathology*, *180*(3), 1136–1144.
817 https://doi.org/10.1016/j.ajpath.2011.12.006
818 Fu, X.-D., & Ares, M. (2014). Context-dependent control of alternative splicing by RNA-binding
819 proteins. *Nature Reviews Genetics*, *15*(10), 689–701. https://doi.org/10.1038/nrg3778
820 Fu, X.-D., & Maniatis, T. (1990). Factor required for mammalian spliceosome assembly is
821 localized to discrete regions in the nucleus. *Nature*, *343*(6257), 437–441.
822 https://doi.org/10.1038/343437a0

Garcias, G. D. L., & Roth, M. D. G. M. (2007). A Brazilian family with quadrupedal gait, severe mental retardation, coarse facial characteristics, and hirsutism. *International Journal of Neuroscience*, *117*(7), 927–933. https://doi.org/10.1080/00207450600910721

Gohr, A., & Irimia, M. (2019). *Matt*: Unix tools for alternative splicing analysis. *Bioinformatics*, *35*(1), 130–132. https://doi.org/10.1093/bioinformatics/bty606

Gulsuner, S., Tekinay, A. B., Doerschner, K., Boyaci, H., Bilguvar, K., Unal, H., Ors, A., Onat, O. E., Atalar, E., Basak, A. N., Topaloglu, H., Kansu, T., Tan, M., Tan, U., Gunel, M., & Ozcelik, T. (2011). Homozygosity mapping and targeted genomic sequencing reveal the gene responsible for cerebellar hypoplasia and quadrupedal locomotion in a consanguineous kindred. *Genome Research*, *21*(12), 1995-2003. https://doi.org/10.1101/gr.126110.111

Haward, F., Maslon, M. M., Yeyati, P. L., Bellora, N., Hansen, J. N., Aitken, S., Lawson, J., von Kriegsheim, A., Wachten, D., Mill, P., Adams, I. R., & Caceres, J. F. (2021). Nucleo-cytoplasmic shuttling of splicing factor SRSF1 is required for development and cilia function. *eLife*, *10*, e65104. https://doi.org/10.7554/eLife.65104

He, F., & Soriano, P. (2013). A critical role for PDGFRα signaling in medial nasal process development. *PLoS Genetics, 9*(9), e1003851. https://doi.org/10.1371/journal.pgen.1003851

Howard, J. M., & Sanford, J. R. (2015). The RNAissance family: SR proteins as multifaceted regulators of gene expression: *Wiley Interdisciplinary Reviews: RNA*, *6*(1), 93–110. https://doi.org/10.1002/wrna.1260

Huang, Y., Yario, T. A., & Steitz, J. A. (2004). A molecular link between SR protein dephosphorylation and mRNA export. *Proceedings of the National Academy of Sciences*, *101*(26), 9666–9670. https://doi.org/10.1073/pnas.0403533101

Jourdain, A. A., Begg, B. E., Mick, E., Shah, H., Calvo, S. E., Skinner, O. S., Sharma, R., Blue, S. M., Yeo, G. W., Burge, C. B., & Mootha, V. K. (2021). Loss of LUC7L2 and U1 snRNP

849 subunits shifts energy metabolism from glycolysis to OXPHOS. *Molecular Cell*, *81*(9),
850 1905-1919.e12. https://doi.org/10.1016/j.molcel.2021.02.033
851 Jumaa, H., Wei, G., & Nielsen, P. J. (1999). Blastocyst formation is blocked in mouse embryos
852 lacking the splicing factor SRp20. *Current Biology*, *9*(16), 899–902.
853 https://doi.org/10.1016/S0960-9822(99)80394-7
854 Klinghoffer, R. A., Hamilton, T. G., Hoch, R., & Soriano, P. (2002). An Allelic Series at the
855 PDGFaR Locus Indicates Unequal Contributions of Distinct Signaling Pathways During
856 Development. *Developmental Cell*, *2*(1), 103–113. https://doi.org/10.1016/s1534-
857 5807(01)00103-4
858 Krainer, R., Mayeda, A., & Kozak, D. (1991). Functional Expression of Cloned Human Splicing
859 Factor SF2: Homology to RNA-Binding Proteins, Ul 70K, and Drosophila Splicing
860 Regulators. *Cell*, *66*(2), 383–394. https://doi.org/10.1016/0092-8674(91)90627-b
861 Kuleshov, M. V., Jones, M. R., Rouillard, A. D., Fernandez, N. F., Duan, Q., Wang, Z., Koplev,
862 S., Jenkins, S. L., Jagodnik, K. M., Lachmann, A., McDermott, M. G., Monteiro, C. D.,
863 Gundersen, G. W., & Ma'ayan, A. (2016). Enrichr: A comprehensive gene set
864 enrichment analysis web server 2016 update. *Nucleic Acids Research*, *44*(W1), W90–
865 W97. https://doi.org/10.1093/nar/gkw377
866 Lee, S., Sears, M. J., Zhang, Z., Li, H., Salhab, I., Krebs, P., Xing, Y., Nah, H.-D., Williams, T., &
867 Carstens, R. P. (2020). Cleft lip and cleft palate in *Esrp1* knockout mice is associated
868 with alterations in epithelial-mesenchymal crosstalk. *Development*, *147*(21), dev187369.
869 https://doi.org/10.1242/dev.187369
870 Li, D., & Roberts, R. (2001). WD-repeat proteins: Structure characteristics, biological function,
871 and their involvement in human diseases. *Cellular and Molecular Life Sciences*, *58*(14),
872 2085-2097. https://doi.org/10.1007/pl00000838

873 Liao, X., Hu, K., Salhi, A., Zou, Y., Wang, J., & Gao, X. (2022). msRepDB: A comprehensive
874 repetitive sequence database of over 80 000 species. *Nucleic Acids Research*, *50*(D1),
875 D236–D245. https://doi.org/10.1093/nar/gkab1089
876 Licatalosi, D. D., & Darnell, R. B. (2010). RNA processing and its regulation: Global insights into
877 biological networks. *Nature Reviews Genetics*, *11*(1), 75–87.
878 https://doi.org/10.1038/nrg2673
879 Liu, K., Jian, Y., Sun, X., Yang, C., Gao, Z., Zhang, Z., Liu, X., Li, Y., Xu, J., Jing, Y., Mitani, S.,
880 He, S., & Yang, C. (2016). Negative regulation of phosphatidylinositol 3-phosphate
881 levels in early-to-late endosome conversion. *Journal of Cell Biology, 212*(2), 181-198.
882 https://doi.org/10.1083/jcb.201506081.
883 Long, Y., Sou, W. H., Yung, K. W. Y., Liu, H., Wan, S. W. C., Li, Q., Zeng, C., Law, C. O. K.,
884 Chan, G. H. C., Lau, T. C. K., & Ngo, J. C. K. (2019). Distinct mechanisms govern the
885 phosphorylation of different SR protein splicing factors. *Journal of Biological Chemistry*,
886 *294*(4), 1312–1327. https://doi.org/10.1074/jbc.RA118.003392
887 Love, M. I., Huber, W., & Anders, S. (2014). Moderated estimation of fold change and
888 dispersion for RNA-seq data with DESeq2. *Genome Biology*, *15*(12), 550.
889 https://doi.org/10.1186/s13059-014-0550-8
890 Mai, C. T., Isenburg, J. L., Canfield, M. A., Meyer, R. E., Correa, A., Alverson, C. J., Lupo, P. J.,
891 Riehle-Colarusso, T., Cho, S. J., Aggarwal, D., Kirby, R. S., & National Birth Defects
892 Prevention Network. (2019). National population-based estimates for major birth defects,
893 2010–2014. *Birth Defects Research*, *111*(18), 1420–1435.
894 https://doi.org/10.1002/bdr2.1589
895 Manning, B. D., & Cantley, L. C. (2007). AKT/PKB Signaling: Navigating Downstream. *Cell*,
896 *129*(7), 1261–1274. https://doi.org/10.1016/j.cell.2007.06.009
897 Martin, M. (2011). Cutadapt removes adapter sequences from high-throughput sequencing
898 reads. *EMBnet.Journal*, *17*(1), 10. https://doi.org/10.14806/ej.17.1.200

899 Miura, Y., Hongu, T., Yamauchi, Y., Funakoshi, Y., Katagiri, N., Ohbayashi, N., & Kanaho, Y.
900 (2016). ACAP3 regulates neurite outgrowth through its GAP activity specific to Arf6 in
901 mouse hippocampal neurons. *Biochemical Journal*, *473*(17), 2591-2602.
902 https://doi.org/10.1042/BCJ20160183
903 Moss, N. D., Wells, K. L., Theis, A., Kim, Y.-K., Spigelman, A. F., Liu, X., MacDonald, P. E., &
904 Sussel, L. (2023). Modulation of insulin secretion by RBFOX2-mediated alternative
905 splicing. *Nature Communications*, *14*(1), 7732. https://doi.org/10.1038/s41467-023-
906 43605-4
907 Pan, Q., Shai, O., Lee, L. J., Frey, B. J., & Blencowe, B. J. (2008). Deep surveying of alternative
908 splicing complexity in the human transcriptome by high-throughput sequencing. *Nature*
909 *Genetics*, *40*(12), 1413–1415. https://doi.org/10.1038/ng.259
910 Park, J. W., Jung, S., Rouchka, E. C., Tseng, Y-T., & Xing, Y. (2016). rMAPS: RNA map
911 analysis and plotting server for alternative exon regulation. *Nucleic Acids Research*
912 *44*(W1), 333-338. https://doi.org/10.1093/nar/gkw410
913 Patro, R., Duggal, G., Love, M. I., Irizarry, R. A., & Kingsford, C. (2017). Salmon provides fast
914 and bias-aware quantification of transcript expression. *Nature Methods*, *14*(4), 417–419.
915 https://doi.org/10.1038/nmeth.4197
916 Ramírez, F., Ryan, D. P., Grüning, B., Bhardwaj, V., Kilpert, F., Richter, A. S., Heyne, S.,
917 Dündar, F., & Manke, T. (2016). deepTools2: A next generation web server for deep-
918 sequencing data analysis. *Nucleic Acids Research*, *44*(W1), W160–W165.
919 https://doi.org/10.1093/nar/gkw257
920 Rapiteanu, R., Davis, L. J., Williamson, J. C., Timms, R. T., Paul Luzio, J., & Lehner, P. J.
921 (2016). A Genetic Screen Identifies a Critical Role for the WDR81-WDR91 Complex in
922 the Trafficking and Degradation of Tetherin. *Traffic*, *17*(8), 940–958.
923 https://doi.org/10.1111/tra.12409

924 Rattanasopha, S., Tongkobpetch, S., Srichomthong, C., Siriwan, P., Suphapeetiporn, K., &
925 Shotelersuk, V. (2012). PDGFRa mutations in humans with isolated cleft palate.
926 *European Journal of Human Genetics*, *20*(10), 1058–1062.
927 https://doi.org/10.1038/ejhg.2012.55
928 Riemondy, K. A., Sheridan, R. M., Gillen, A., Yu, Y., Bennett, C. G., & Hesselberth, J. R. (2017).
929 valr: Reproducible genome interval analysis in R. *F1000Research*, *6*, 1025.
930 https://doi.org/10.12688/f1000research.11997.1
931 Robinson, J. T., Thorvaldsdóttir, H., Winckler, W., Guttman, M., Lander, E. S., Getz, G., &
932 Mesirov, J. P. (2011). Integrative genomics viewer. *Nature Biotechnology*, *29*(1), 24–26.
933 https://doi.org/10.1038/nbt.1754
934 Rogers, M. A., Campaña, M. B., Long, R., & Fantauzzo, K. A. (2022). PDGFR dimer-specific
935 activation, trafficking and downstream signaling dynamics. *Journal of Cell Science*,
936 *135*(17), jcs259686. https://doi.org/10.1242/jcs.259686
937 Schmok, J. C., Jain, M., Street, L. A., Tankka, A. T., Schafer, D., Her, H.-L., Elmsaouri, S.,
938 Gosztyla, M. L., Boyle, E. A., Jagannatha, P., Luo, E.-C., Kwon, E. J., Jovanovic, M., &
939 Yeo, G. W. (2024). Large-scale evaluation of the ability of RNA-binding proteins to
940 activate exon inclusion. *Nature Biotechnology*. https://doi.org/10.1038/s41587-023-
941 02014-0
942 Scotti, M. M., & Swanson, M. S. (2016). RNA mis-splicing in disease. *Nature Reviews Genetics*,
943 *17*(1), 19–32. https://doi.org/10.1038/nrg.2015.3
944 Shen, H., & Green, M. R. (2006). RS domains contact splicing signals and promote splicing by a
945 common mechanism in yeast through humans. *Genes & Development*, *20*(13), 1755–
946 1765. https://doi.org/10.1101/gad.1422106
947 Shen, S., Park, J. W., Lu, Z., Lin, L., Henry, M. D., Wu, Y. N., Zhou, Q., & Xing, Y. (2014).
948 rMATS: Robust and flexible detection of differential alternative splicing from replicate

RNA-Seq data. *Proceedings of the National Academy of Sciences*, *111*(51), E5593–E5601. https://doi.org/10.1073/pnas.1419161111

Shin, C., Feng, Y., & Manley, J. L. (2004). Dephosphorylated SRp38 acts as a splicing repressor in response to heat shock. *Nature*, *427*(6974), 553–558. https://doi.org/10.1038/nature02288

Simpson, J. E., Muir, M. T., Lee, M., Naughton, C., Gilbert, N., Pollard, S. M., & Gammoh, N. (2024). Autophagy supports PDGFRA-dependent brain tumor development by enhancing oncogenic signaling. *Developmental Cell*, S1534580723006214. https://doi.org/10.1016/j.devcel.2023.11.023

Soneson, C., Love, M. I., & Robinson, M. D. (2016). Differential analyses for RNA-seq: Transcript-level estimates improve gene-level inferences [version 2; referees: 2 approved]. *F1000Research*, *4*, 1521. https://doi.org/10.12688/F1000RESEARCH.7563.2

Soriano, P. (1997). The PDGFα receptor is required for neural crest cell development and for normal patterning of the somites. *Development*, *124*(14), 2691–2700. https://doi.org/10.1242/dev.124.14.2691

Tallquist, M. D., & Soriano, P. (2003). Cell autonomous requirement for PDGFRα in populations of cranial and cardiac neural crest cells. *Development*, *130*(3), 507–518. https://doi.org/10.1242/dev.00241

Uyar, B., Yusuf, D., Wurmus, R., Rajewsky, N., Ohler, U., & Akalin, A. (2017). RCAS: An RNA centric annotation system for transcriptome-wide regions of interest. *Nucleic Acids Research*, *45*(10), e91–e91. https://doi.org/10.1093/nar/gkx120

Van Nostrand, E. L., Nguyen, T. B., Gelboin-Burkhart, C., Wang, R., Blue, S. M., Pratt, G. A., Louie, A. L., & Yeo, G. W. (2017). Robust, Cost-Effective Profiling of RNA Binding Protein Targets with Single-end Enhanced Crosslinking and Immunoprecipitation

(seCLIP). In Y. Shi (Ed.), *mRNA Processing* (Vol. 1648, pp. 177–200). Springer New York. https://doi.org/10.1007/978-1-4939-7204-3_14

Van Nostrand, E. L., Pratt, G. A., Shishkin, A. A., Gelboin-Burkhart, C., Fang, M. Y., Sundararaman, B., Blue, S. M., Nguyen, T. B., Surka, C., Elkins, K., Stanton, R., Rigo, F., Guttman, M., & Yeo, G. W. (2016). Robust transcriptome-wide discovery of RNA-binding protein binding sites with enhanced CLIP (eCLIP). *Nature Methods*, *13*(6), 508–514. https://doi.org/10.1038/nmeth.3810

Vasudevan, H. N., Mazot, P., He, F., & Soriano, P. (2015). Receptor tyrosine kinases modulate distinct transcriptional programs by differential usage of intracellular pathways. *eLife*, *4*, e07186. https://doi.org/10.7554/eLife.07186

Wallroth, A., & Haucke, V. (2018). Phosphoinositide conversion in endocytosis and the endolysosomal system. *Journal of Biological Chemistry*, *293*(5), 1526–1535. https://doi.org/10.1074/jbc.R117.000629

Wang, E. T., Sandberg, R., Luo, S., Khrebtukova, I., Zhang, L., Mayr, C., Kingsmore, S. F., Schroth, G. P., & Burge, C. B. (2008). Alternative isoform regulation in human tissue transcriptomes. *Nature*, *456*(7221), 470–476. https://doi.org/10.1038/nature07509

Xiao, S. H., & Manley, J. (1997). Phosphorylation of the ASF/SF2 RS domain affects both protein-protein and protein-RNA interactions and is necessary for splicing. *Genes & Development*, *11*(3), 334-344. https://doi.org/10.1101/gad.11.3.334

Yee, B. A., Pratt, G. A., Graveley, B. R., Van Nostrand, E. L., & Yeo, G. W. (2019). RBP-Maps enables robust generation of splicing regulatory maps. *RNA*, *25*(2), 193-204. https://doi.org/10.1261/rna.069237.118

Yoo, J. H., Brady, S. W., Acosta-Alvarez, L., Rogers, A., Peng, J., Sorensen, L. K., Wolff, R. K., Mleynek, T., Shin, D., Rich, C. P., Kircher, D. A., Bild, A., Odelberg, S. J., Li, D. Y., Holmen, S. L., & Grossmann, A. H. (2019). The small GTPase ARG5 activates PI3K in

melanoma to induce a prometastatic state. *Cancer Research, 79*(11), 2892-2908. https://doi.org/10.1158/0008-5472.CAN-18-3026

Zahler, A. M., Neugebauer, K. M., Lane, W. S., & Roth, M. B. (1993). Distinct Functions of SR Proteins in Alternative pre-mRNA Splicing. *Science*, *260*(5105), 219–222. https://doi.org/10.1126/science.8385799

Zerial, M., & McBride, H. (2001). Rab proteins as membrane organizers. *Nature Reviews Molecular Cell Biology*, *2*(2), 107–117. https://doi.org/10.1038/35052055

Zhou, Z., & Fu, X.-D. (2013). Regulation of splicing by SR proteins and SR protein-specific kinases. *Chromosoma*, *122*(3), 191–207. https://doi.org/10.1007/s00412-013-0407-z

Zhou, Z., Qiu, J., Liu, W., Zhou, Y., Plocinik, R. M., Li, H., Hu, Q., Ghosh, G., Adams, J. A., Rosenfeld, M. G., & Fu, X.-D. (2012). The Akt-SRPK-SR Axis Constitutes a Major Pathway in Transducing EGF Signaling to Regulate Alternative Splicing in the Nucleus. *Molecular Cell*, *47*(3), 422–433. https://doi.org/10.1016/j.molcel.2012.05.014

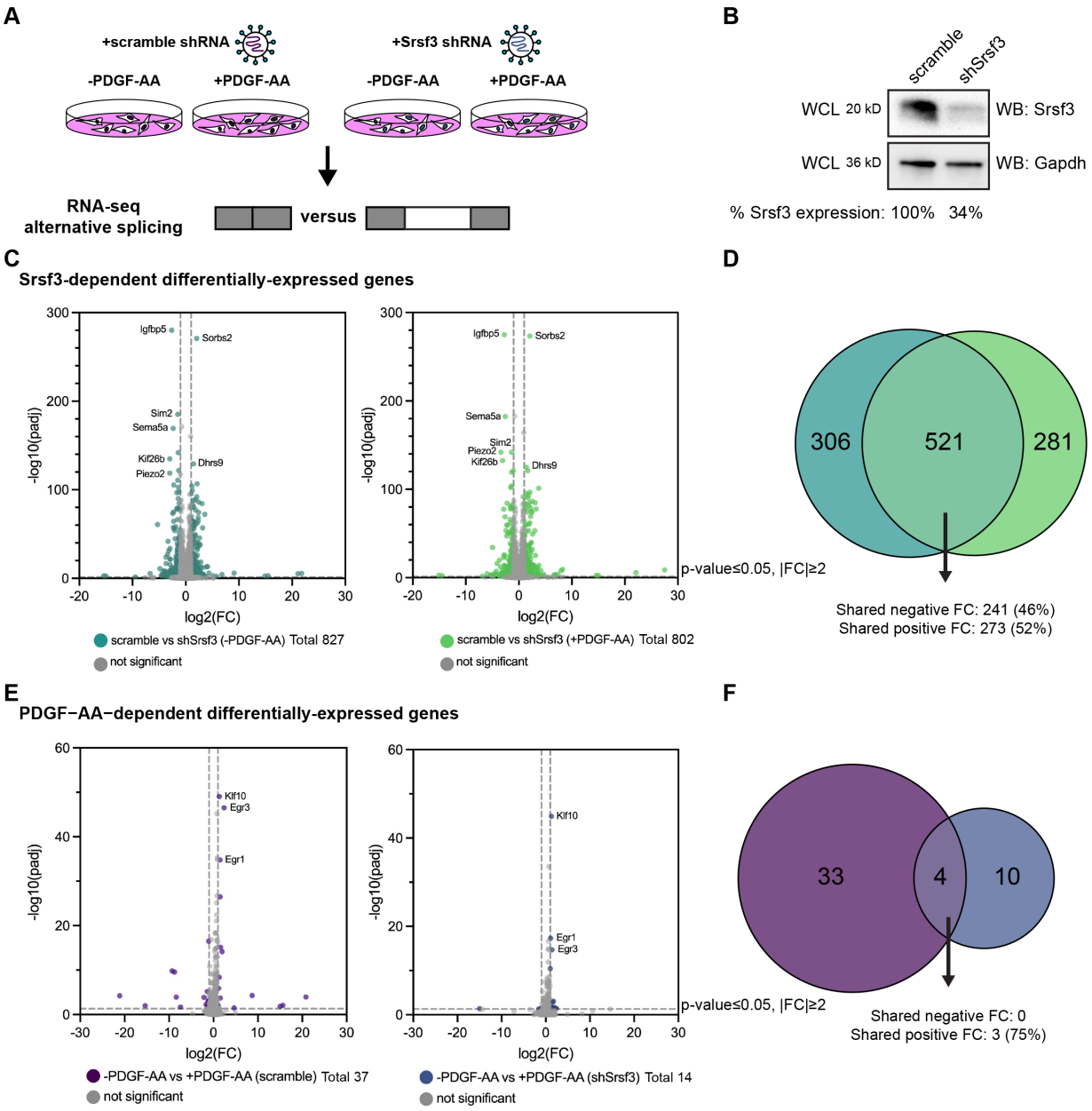

Figure 1: PDGFRα signaling for one hour minimally affects gene expression. (A) Schematic of RNA-seq experimental design. iMEPM cells were transduced to stably express a scramble shRNA (scramble) or shRNA targeting the 3' UTR of *Srsf3* (shSrsf3). iMEPM cells expressing either scramble or shSrsf3 were left unstimulated or stimulated with 10 ng/mL PDGF-AA for 1 hour and RNA was isolated for RNA-seq analysis. **(B)** Western blot (WB) analysis of whole-cell lysates (WCL) from scramble and shSrsf3 cell lines with anti-Srsf3 and

anti-Gapdh antibodies. The percentage of Srsf3 expression normalized to Gapdh expression is indicated below. **(C)** Volcano plots depicting differentially-expressed genes in scramble versus shSrsf3 cell lines in the absence (left) or presence (right) of PDGF-AA stimulation. Log_2(fold change) (FC) values represent log_2(shSrsf3 normalized counts/scramble normalized counts). Significant changes in gene-level expression are reported for genes with adjusted *P* (padj) < 0.05 and fold change |FC| ≥ 2. **(D)** Venn diagram of significant genes from C. **(E)** Volcano plots depicting differentially-expressed genes in the absence versus presence of PDGF-AA ligand in scramble (left) or shSrsf3 (right) cell lines. Log_2(FC) values represent log_2(+PDGF-AA normalized counts/-PDGF-AA normalized counts). **(F)** Venn diagram of significant genes from E.

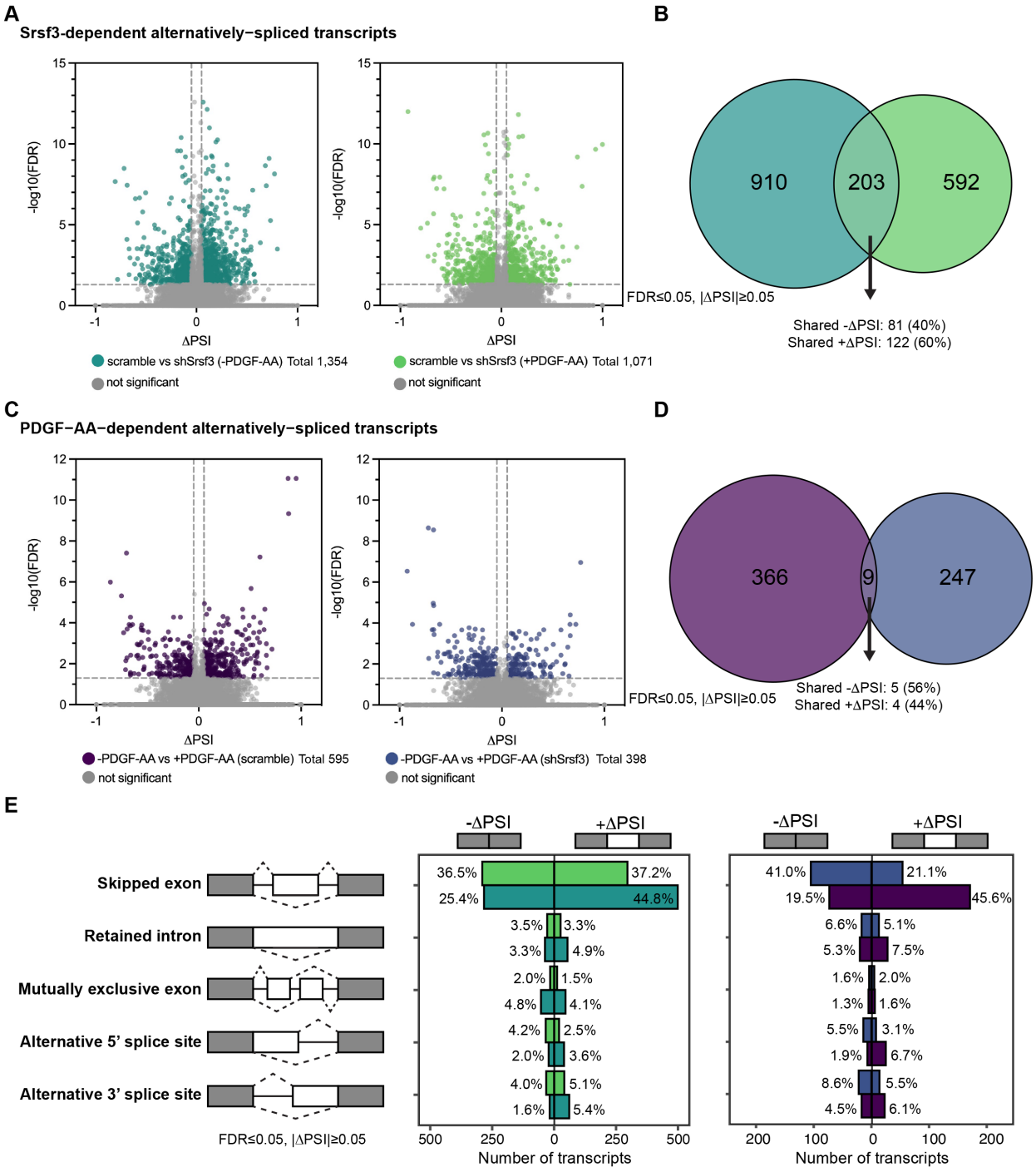

Figure 2: PDGFRα signaling for one hour has a more pronounced effect on alternative RNA splicing. (A) Volcano plots depicting alternatively-spliced transcripts in scramble versus shSrsf3 cell lines in the absence (left) or presence (right) of PDGF-AA stimulation. Difference in percent spliced in (ΔPSI) values represent scramble PSI – shSrsf3 PSI. Significant changes in

alternative RNA splicing are reported for events with a false discovery rate (FDR) ≤ 0.05 and a difference in percent spliced in (|ΔPSI|) ≥ 0.05. **(B)** Venn diagram of significant transcripts from A, filtered to include events detected in at least 10 reads in either condition. **(C)** Volcano plots depicting alternatively-spliced transcripts in the absence versus presence of PDGF-AA ligand in scramble (left) or shSrsf3 (right) cell lines. Difference in percent spliced in (ΔPSI) values represent -PDGF-AA PSI – +PDGF-AA PSI. **(D)** Venn diagram of significant transcripts from C, filtered to include events detected in at least 10 reads in either condition. **(E)** Bar graphs depicting alternative RNA splicing events in scramble versus shSrsf3 cell lines in the absence or presence of PDGF-AA stimulation (left) or in the absence versus presence of PDGF-AA ligand in scramble or shSrsf3 cell lines (right).

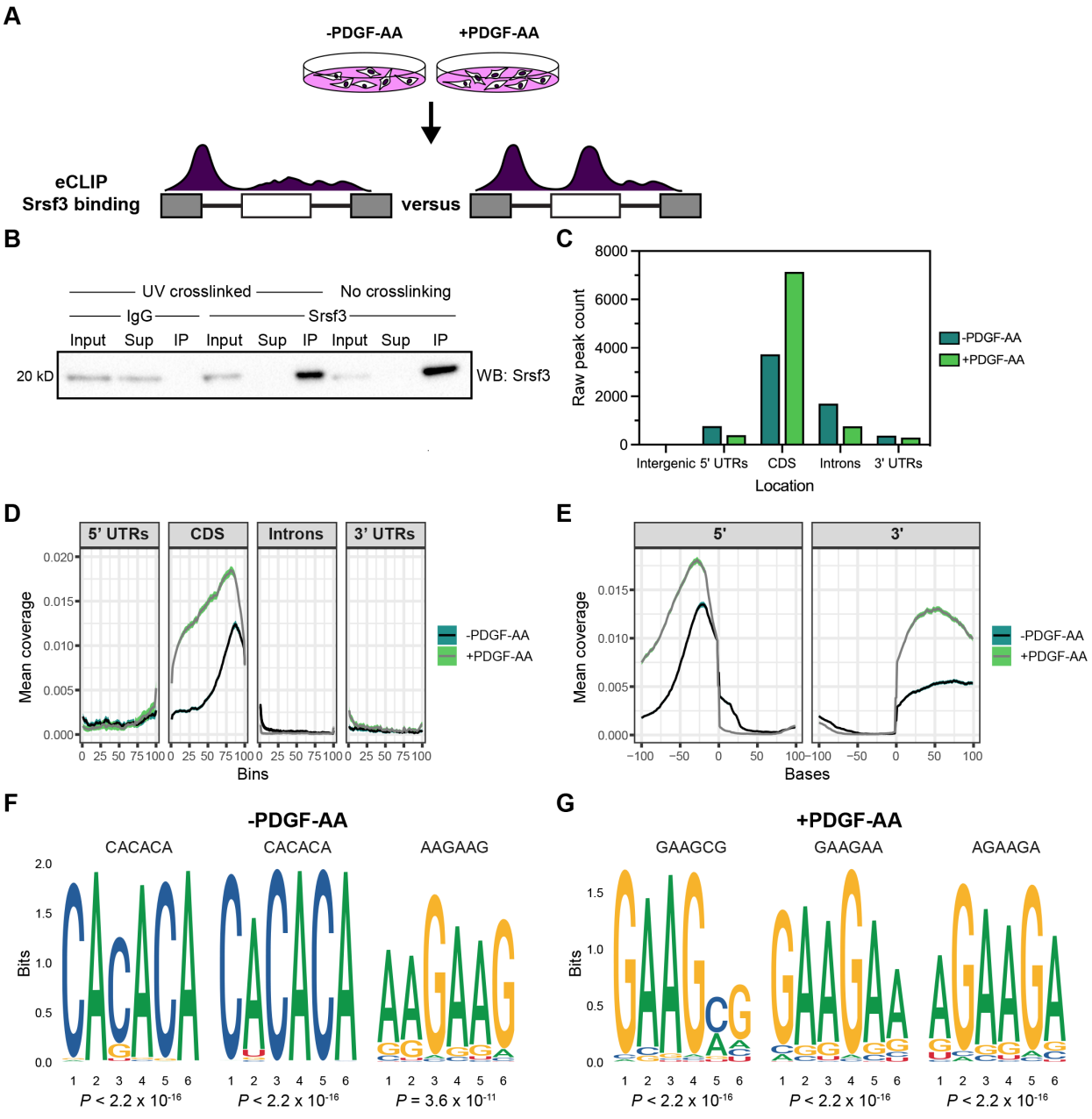

Figure 3: Srsf3 exhibits differential transcript binding upon PDGFRα signaling. (A) Schematic of eCLIP experimental design. iMEPM cells were left unstimulated or stimulated with 10 ng/mL PDGF-AA for 1 hour and processed for eCLIP analysis. **(B)** Immunoprecipitation (IP) of Srsf3 from cells that were UV-crosslinked or not UV-crosslinked with IgG or an anti-Srsf3 antibody followed by western blotting (WB) of input, supernatant (Sup), and IP samples with an anti-Srsf3 antibody. **(C)** Mapping of eCLIP peaks to various transcript locations in the absence

or presence of PDGF-AA stimulation. 5' UTR, 5' untranslated region; CDS, coding sequence; 3' UTR, 3' untranslated region. **(D,E)** Mean coverage of eCLIP peaks across various transcript locations (D) and surrounding the 5' and 3' splice sites (E) in the absence or presence of PDGF-AA stimulation. **(F,G)** Top three motifs enriched in eCLIP peaks in the absence (F) or presence (G) of PDGF-AA stimulation with associated *P* values.

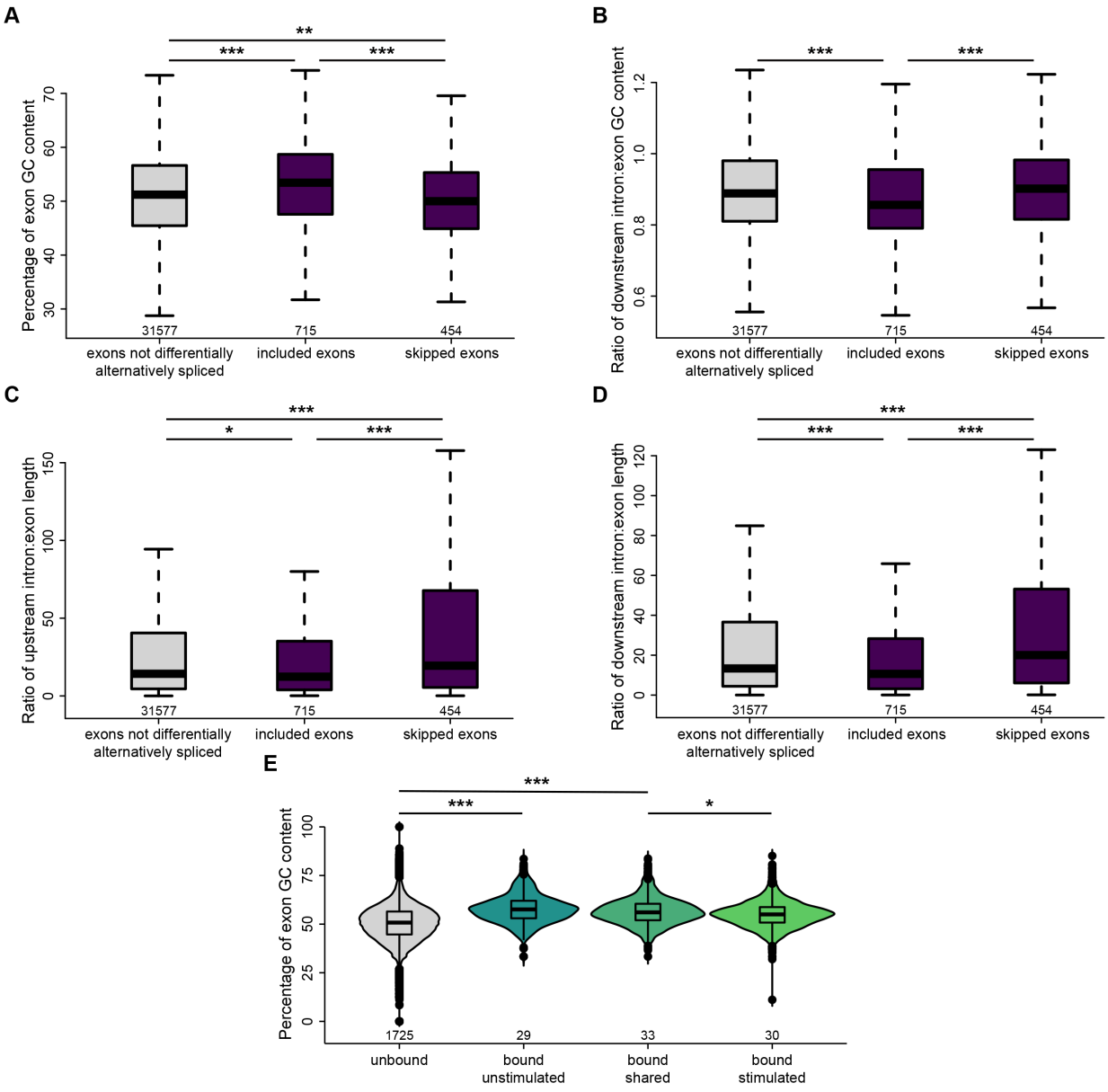

Figure 4: Srsf3 and PDGFRα signaling are associated with differential GC content and length of alternatively-spliced exons. (A) Box and whisker plot depicting the percentage of exon GC content in exons that are not differentially alternatively spliced, and exons that are included or skipped when Srsf3 is present from the rMATS analysis. **(B)** Box and whisker plot depicting the ratio of downstream intron to exon GC content in exons that are not differentially alternatively spliced, and exons that are included or skipped when Srsf3 is present from the rMATS analysis. **(C,D)** Box and whisker plots depicting the ratio of upstream intron to exon

length (C) and downstream intron to exon length (D) in exons that are not differentially alternatively spliced, and exons that are included or skipped when Srsf3 is present from the rMATS analysis. **(E)** Violin and box and whisker (inset) plots depicting the percentage of exon GC content in exons that are not bound by Srsf3, and exons that are bound in the absence and/or presence of PDGF-AA stimulation from the eCLIP analysis. *, $P < 0.05$; **, $P < 0.01$; ***, $P < 0.001$.

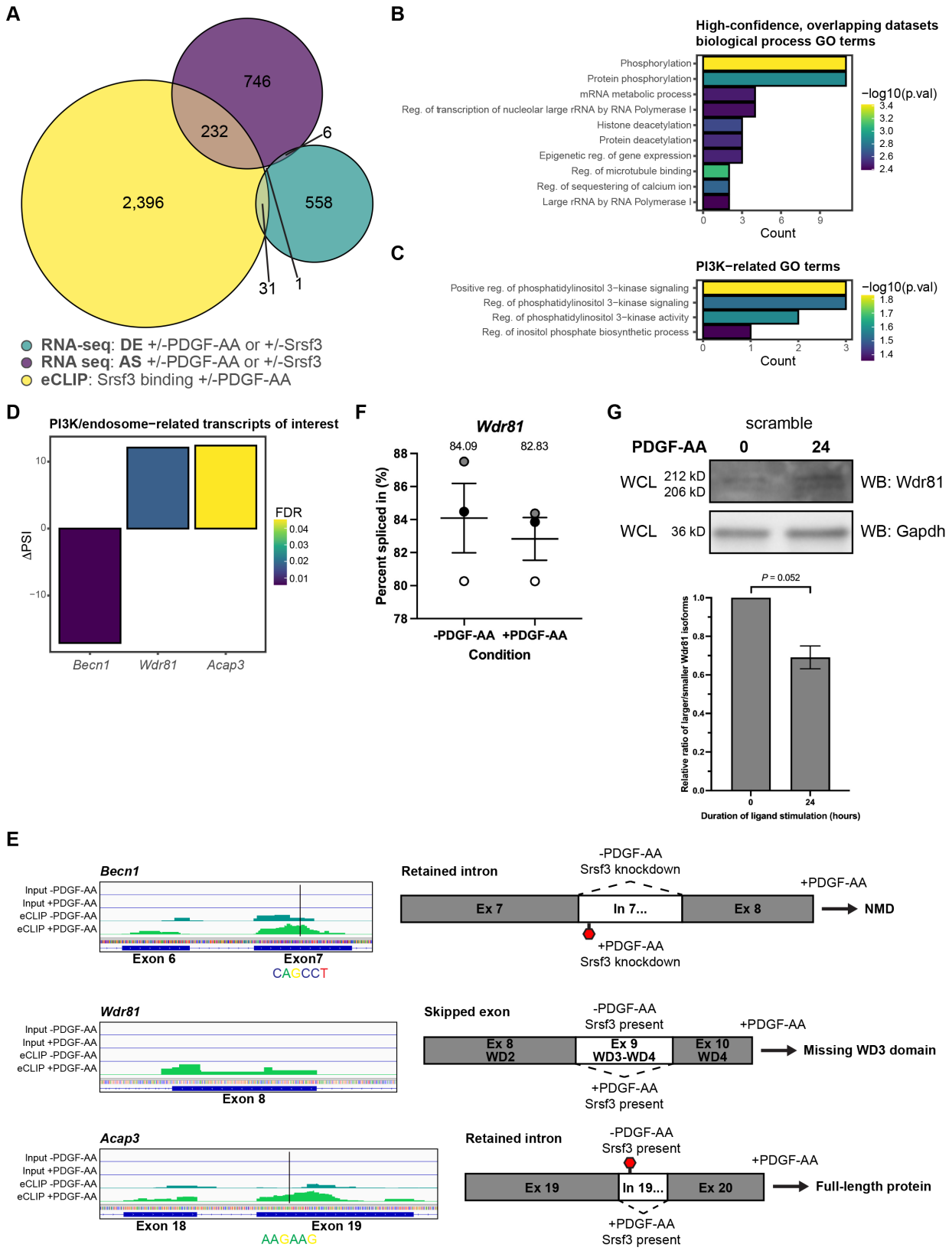

Figure 5: Transcripts bound by Srsf3 that undergo alternative splicing upon PDGFRα signaling encode regulators of PI3K signaling. (A) Venn diagram of genes with differential expression (DE) or transcripts subject to alternative RNA splicing (AS) across the four treatment comparisons that overlap with transcripts with Srsf3 eCLIP peaks in the absence or presence of PDGF-AA stimulation. **(B,C)** Top ten (B) and PI3K-related (C) biological process gene ontology (GO) terms for transcripts from the high-confidence, overlapping datasets. p.val, *P*. **(D)** Difference in percent spliced in (ΔPSI) values for PI3K/endosome-related transcripts of interest. ΔPSI values represent -PDGF-AA PSI – +PDGF-AA PSI. FDR, false detection rate. **(E)** Peak visualization for input and eCLIP samples in the absence or presence of PDGF-AA stimulation from Integrative Genomics Viewer (left) with location of motifs from Figure S6 indicated below for PI3K/endosome-related transcripts of interest. Predicted alternative splicing outcomes for PI3K/endosome-related transcripts of interest (right). **(F)** Scatter dot plot depicting the percent spliced in as assessed by qPCR analysis of *Wdr81* exon 9 in the scramble cell line following 1 h of PDGF-AA stimulation quantified from $n = 3$ biological replicates. Data are mean ± s.e.m. Shaded circles correspond to independent experiments. **(G)** Western blot (WB) analysis of whole-cell lysates (WCL) from the scramble cell line following 24 h of PDGF-AA stimulation with anti-Wdr81 and anti-Gapdh antibodies. Bar graph depicting relative ratios of larger/smaller Wdr81 isoforms quantified from $n = 3$ biological replicates as above. Data are mean ± s.e.m.

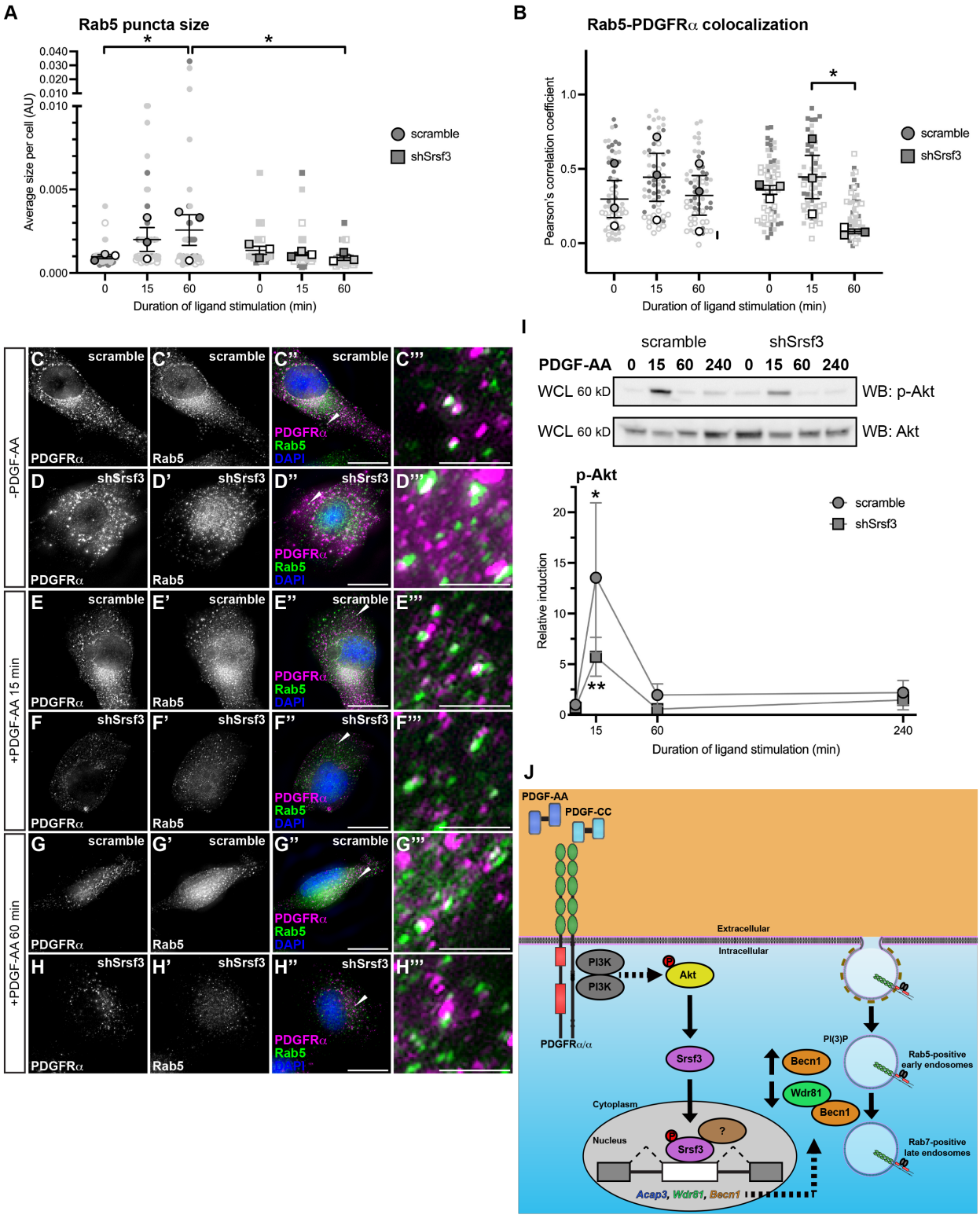

Figure 6: Srsf3 regulates early endosome size and phosphorylation of Akt downstream of PDGFRα signaling. (A,B) Scatter dot plots depicting average size of Rab5 puncta per cell (A)

and Pearson's correlation coefficient of signals from anti-Rab5 and anti-PDGFRα antibodies (B) in scramble and shSrsf3 cell lines in the absence or presence (15-60 min) of PDGF-AA stimulation. Data are mean ± s.e.m. *, $P < 0.05$. Shaded shapes correspond to independent experiments. Summary statistics from biological replicates consisting of independent experiments (large shapes) are superimposed on top of data from all cells; $n = 20$ technical replicates across each of three biological replicates. **(C-H"')** PDGFRα antibody signal (white or magenta) and Rab5 antibody signal (white or green) as assessed by immunofluorescence analysis of scramble and shSrsf3 cells in the absence or presence (15-60 min) of PDGF-AA stimulation. Nuclei were stained with DAPI (blue). White arrows denote regions of colocalization, which are expanded in C"'-H"'. Scale bars: 20 μm (C-H"), 3 μm (C"'-H"'). **(I)** Western blot (WB) analysis of whole-cell lysates (WCL) from scramble (left) and shSrsf3 (right) cell lines following a time course of PDGF-AA stimulation from 15 min to 4 h, with anti-phospho-(p)-Akt and anti-Akt antibodies. Line graph depicting quantification of band intensities from $n = 3$ biological replicates as above. Data are mean ± s.e.m. *, $P < 0.05$; **, $P < 0.01$. **(J)** Model of experimental results in which PI3K/Akt-mediated PDGFRα signaling results in the nuclear translocation of Srsf3 and the subsequent AS of transcripts to decrease levels of proteins that promote PDGFRα trafficking out of early endosomes.